



Spatiotemporal patterns of a diffusive prey-predator model with spatial memory and pregnancy period in an intimidatory environment

Cuihua Wang¹ · Sanling Yuan¹  · Hao Wang²

Received: 8 October 2020 / Revised: 11 September 2021 / Accepted: 5 January 2022

© The Author(s), under exclusive licence to Springer-Verlag GmbH Germany, part of Springer Nature 2022

Abstract

Spatial memory and predator-induced fear have recently been considered in modeling population dynamics of animals independently. This paper is the first to integrate both aspects in a prey-predator model with pregnancy cycle to investigate the direct and indirect effects of predation on the spatial distribution of prey. We extensively study Turing instability and Hopf bifurcation. When the prey population has slow memory-based diffusion, the model is easier to generate Turing patterns. While when the prey population has fast memory-based diffusion, the model can exhibit rich dynamics. Specifically, (1) for the model with spatial memory delay only, the prey population with long term memory shows a spatially nonhomogeneous periodic distribution; (2) for the model with pregnancy delay only, the prey population with long pregnancy cycles shows a spatially homogeneous (or nonhomogeneous) periodic distribution, and (3) for the model with both the two time delays, more interesting spatiotemporal dynamics can be observed for long memory delay and (or) long pregnancy cycles. Our findings indicate that both spatial memory and pregnancy cycle play significant roles in the pattern formation of prey-predator interactions.

Cuihua Wang and Sanling Yuan are supported by National Natural Science Foundation of China (11671260; 12071293); Hao Wang is supported by Natural Sciences and Engineering Research Council of Canada (Discovery Grant RGPIN-2020-03911 and Accelerator Supplement Grant RGPAS-2020-00090).

✉ Sanling Yuan
Sanling@usst.edu.cn
Hao Wang
hao8@ualberta.ca

¹ College of Science, University of Shanghai for Science and Technology, Shanghai 200093, People's Republic of China

² Department of Mathematical and Statistical Sciences, University of Alberta, Edmonton, AB T6G2G1, Canada

Keywords Spatial memory · Predator-induced fear · Pregnancy period · Delay reaction-diffusion equations · Pattern formation · Stability and Hopf bifurcation

Mathematics Subject Classification 92-10 · 92B05 · 92C15

1 Introduction

For nearly a century, the main influence of predators on prey is generally assumed to be the loss of prey by direct predation (Wang et al. 2009; Sun 2016; Shi et al. 2017, 2019; Jia et al. 2019; Wang and Li 2019; Yan et al. 2020; Yang and Yuan 2021; Zhang et al. 2022). Recently, Montagnes et al. (2019) pointed out that ignoring the biological aspects of predators and prey behind predation may cause a ‘false exclusion’. Some convincing experimental studies demonstrated that the exposure of predators or predator cues can have a sustained effects on foraging, food intake and the physiological condition of prey (Clinchy et al. 2013; Zanette et al. 2011; Travers et al. 2010; Preisser et al. 2005). For instance, Preisser et al. (2005) indicated that the impact of intimidation on prey is at least as strong as direct killing and the costs of intimidation may actually be the dominant facet of trophic interactions. Zanette et al. (2011) found that the predator-induced fear may give rise to the decrease of the birth rate and survival rate of prey’s offsprings.

Generally speaking, one can understand the quantitative effect of predator-induced fear on the population dynamics of prey through aforementioned experimental studies. In terms of the qualitative influence, it needs to be discussed through mathematical modeling. Wang et al. (2016) originally introduced the cost of fear on prey into the classical Lotka-Volterra model by multiplying the growth term by a fear factor. Their results revealed that the direction of Hopf bifurcation will change as the fear level increases, which enriches the results of the typical supercritical Hopf bifurcation for classical prey-predator models. Soon afterwards, Wang and Zou (2017) uncovered that the anti-predation behavior of adult prey is positively correlated with the prey density but negatively correlated with the fear intensity by constituting a stage structure model with maturation delay. Readers are also referred to Wang and Zou (2020), Mondal et al. (2018), Kumar and Dubey (2019) and the references therein for more related works on this respect.

The models mentioned above are all ordinary or delayed differential equation systems independent of individual movement. Actually, no individuals are static and they always move over space. As a result, when prey are threatened by predators, they may escape from predators by showing various anti-predator behaviors and then predators want to pursue prey. In other words, prey may move oppositely to the gradient of the predators and such movement can be described by predator-taxis. Based on this, Wang and Zou (2018) further proposed a reaction-diffusion prey-predator model with anti-predator behaviors and they found that for Holling-II functional response function, small predator-taxis rate may induce pattern formation.

In addition, spatial memory may bring many benefits to animals, including improved choice of key locations such as food storage, nesting places, etc. (Fagan et al. 2013; Potts and Lewis 2019). Lately, Fagan et al. (2013) pointed out that it is necessary to

combine the spatial memory with spatial mobility. The ability to perceive risks for animals is related not only to the environment, but also to previous exposure to risks and their memory ability. A natural question arising is how spatial memory changes the spatial movement patterns or spatial distributions of animals? Recently, some scholars have paid attention to this problem and carried out some related research works (Shi et al. 2020; Song et al. 2019, 2021). Shi et al. (2020) originally proposed a minimal self-contained single species model to incorporate spatial memory using a modified Fick's law, and the model has the form of a reaction-diffusion equation with a delayed diffusion term. Song et al. (2019) proposed a single species model with memory-based diffusion and nonlocal interaction and found that the interaction of memory delay and diffusion may result in the occurrence of Turing-Hopf and double Hopf bifurcations. However, to our knowledge, despite the surging interest in the role of spatial memory, few attention has been paid to the influence of spatial memory on the spatial distribution for the species living in an intimidatory environment. Motivated by the technique used in Shi et al. (2020), this paper explicitly includes the spatial memory as a time delay into the predator-prey model proposed in Wang and Zou (2018) to explore how it affects the spatial distribution of prey.

On the other hand, as mentioned in Clinchy et al. (2013) and Wang et al. (2016), the predator-induced fear may have an extremely harmful impact on the survival quality of the prey population, which encompasses the decrease of the birth rate, the increase of the death rate, and the deteriorated psychological condition of juveniles, etc. Especially, for a species under consideration, due to the particularity of the pregnant individuals, the impact of fear factors on them will be magnified many times. In mathematical modeling, the pregnancy cycle is usually introduced by considering as a time delay, which has been used to reveal many interesting natural phenomena (May 1973; Martin and Ruan 2001). In this paper, we also follow the same way to introduce the pregnancy cycle of prey into our model to discuss its impact on the spatial distribution of prey in a intimidatory environment.

The prey-predator model proposed in this paper presents a reaction-diffusion equations model with a delayed chemotaxis term and a pregnancy delay. Our results show that spatial memory, pregnancy cycle as well as memory-based diffusion and fear level all affect the spatial distribution of the population to varying degrees. The organization of this paper is arranged as follows. The detailed derivation process of the studied model (3) is presented in Sect. 2. In Sect. 3, we address the existence and stability of constant equilibria for the temporal version of the model. In Sect. 4, we mainly discuss three kinds of solutions for model (3) with or without delays: nonconstant steady-state solutions, spatially homogeneous periodic solutions and spatially nonhomogeneous periodic solutions. Some enlightening numerical simulations are performed in Sect. 5 to observe the influence of memory-based diffusion, spatial memory, pregnancy period and fear level on the spatial distribution of prey. Finally, we summarize and discuss our main results.

2 Model formulation

In this section, we begin with the model considered in Wang and Zou (2018) to propose a new prey-predator model by introducing spatial memory and pregnancy cycle of prey.

Assuming that the prey and predator populations live in an isolated bounded domain Ω with a smooth boundary $\partial\Omega$ and letting $u(x, t)$ and $v(x, t)$ stand respectively for the densities of prey and the predators at position $x \in \Omega$ and time t , Wang and Zou (2018) proposed the following model:

$$\begin{cases} \frac{\partial u}{\partial t} = d_1 \Delta u + \chi \nabla \cdot (\beta(u)u \nabla v) + \frac{ru}{1+kv} - du - au^2 - \frac{puv}{1+cu}, & x \in \Omega, t > 0, \\ \frac{\partial v}{\partial t} = d_2 \Delta v - mv^2 + \frac{quv}{1+cu}, & x \in \Omega, t > 0, \\ \frac{\partial u}{\partial \nu} = 0, \quad \frac{\partial v}{\partial \nu} = 0, & x \in \partial\Omega, t > 0, \\ u(x, 0) = u_0(x) \geq 0, \quad v(x, 0) = v_0(x) \geq 0, & x \in \Omega, \end{cases} \tag{1}$$

where all parameters are assumed to be positive numbers. The parameters r and d are respectively the growth rate and the natural death rate of prey irrespective of the fear cost. The parameters a and m denote respectively the death rates of prey and predators due to intra-specific competition. The predation term is embodied by the Holling-II functional response function accounting for the direct predation. The growth factor $\frac{1}{1+kv}$ stands for the cost of fear from the predators and k measures the level of the fear effect. The chemotaxis term $\chi \nabla \cdot (\beta(u)u \nabla v)$ reflects that the prey individuals tend to lower gradient of the predator density, and here $\beta(u) > 0$ describes the volume filling effect, $\chi > 0$ measures the sensitivity of prey to the predation risk. In the domain Ω , the two species move randomly at the rate of d_1 and d_2 , respectively. At the boundary $\partial\Omega$, the Neumann boundary condition is imposed, which implies that the densities of the prey and predator populations do not change by crossing the boundary. The initial functions $u_0(x)$ and $v_0(x)$ are nonnegative and continuous.

As mentioned in the previous section, spatial memory may have a great impact on the spatial distribution of populations, and such effect is even greater in an intimidatory environment. Suppose that the average memory period of the prey individuals is τ_1 . Arguing similarly as in Shi et al. (2020), spatial memory can be characterized by using a modified Fick’s law in which the flux of prey movement at time t is proportional to its density at time t and the spatial gradient of predators at time $t - \tau_1$. By incorporating this into model (1), we propose the following model:

$$\begin{cases} \frac{\partial u}{\partial t} = d_1 \Delta u + \chi \beta \nabla \cdot (u \nabla v_{\tau_1}) + \frac{ru}{1+kv} - du - au^2 - \frac{puv}{1+cu}, & x \in \Omega, t > 0, \\ \frac{\partial v}{\partial t} = d_2 \Delta v - mv^2 + \frac{quv}{1+cu}, & x \in \Omega, t > 0, \\ \frac{\partial u}{\partial \nu} = 0, \quad \frac{\partial v}{\partial \nu} = 0, & x \in \partial\Omega, t > 0, \\ u(x, t) = u_0(x) \geq 0, \quad v(x, t) = v_0(x) \geq 0, & x \in \Omega, t \in (-\tau_1, 0], \end{cases} \tag{2}$$

where we assume that the individuals live in a vast and bounded environment and ignore the volume filling effect, that is $\beta(u) = \beta$.

Moreover, it seems reasonable to assume that the pregnant prey individuals do not move during their pregnancy cycles. Then the delayed term for the pregnancy period becomes reasonable, avoiding the common modeling issue for a delayed partial differential equation. Here the birth rate of prey at time t is affected by the fear from predators at time $t - \tau_2$, where τ_2 is the average pregnancy period of prey. This is described by the term $\frac{1}{1+kv(x,t-\tau_2)}$, and thus model (2) becomes

$$\begin{cases} \frac{\partial u}{\partial t} = d_1 \Delta u + \alpha \nabla \cdot (u \nabla v_{\tau_1}) + \frac{ru}{1+kv_{\tau_2}} - du - au^2 - \frac{puv}{1+cu}, & x \in \Omega, t > 0, \\ \frac{\partial v}{\partial t} = d_2 \Delta v - mv^2 + \frac{quv}{1+cu}, & x \in \Omega, t > 0, \\ \frac{\partial u}{\partial \nu} = 0, \quad \frac{\partial v}{\partial \nu} = 0, & x \in \partial \Omega, t > 0, \\ u(x, t) = u_0(x) \geq 0, v(x, t) = v_0(x) \geq 0, & x \in \Omega, t \in (-\max\{\tau_1, \tau_2\}, 0], \end{cases} \tag{3}$$

where $v_{\tau_2} = v(x, t - \tau_2)$ and $\alpha = \chi\beta$.

In this paper, we are engrossed in investigating the spatiotemporal dynamics of model (3) to reveal how spatial memory and pregnancy cycles affect the spatiotemporal distribution of prey. Notice that model (3) has two independent time delays. Such models are often encountered in different fields (Cooke and Den Driessche 1996; Jackson and Chencharpentier 2017; Song et al. 2008; Qu et al. 2010; Ruan and Wei 2003; Shi et al. 2019; Du et al. 2019; An et al. 2020). Mathematically, one can consider their dynamics by fixing one delay and varying the other one (Qu et al. 2010; Ruan and Wei 2003). An alternative approach is to exert geometric method to show the properties of stability switching curves (Gu et al. 2005), which has been frequently used to analyze Hopf bifurcations for various models with two delays (Lin and Wang 2012; An et al. 2019; Shi et al. 2019). In this paper, we will apply this approach to explore the properties of the critical curves of Hopf bifurcations for model (3) with $\tau_1, \tau_2 > 0$.

3 Temporal prey-predator model

The nonspatial version of model (3) in the absence of delays is

$$\begin{cases} \frac{du}{dt} = \frac{ru}{1+kv} - du - au^2 - \frac{puv}{1+cu}, \\ \frac{dv}{dt} = -mv^2 + \frac{quv}{1+cu}. \end{cases} \tag{4}$$

The equilibria of model (4), or the constant steady state of model (3), can be determined by letting $\frac{du}{dt} = 0$ and $\frac{dv}{dt} = 0$. Obviously, model (4) always exists the trivial equilibrium $(0, 0)$, which is unique provided $r \leq d$. When $r > d$, a semi-trivial equi-

librium $(\frac{r-d}{a}, 0)$ emerges. Any positive equilibrium (u^*, v^*) of model (4), if exists, must satisfy $v^* = \frac{qu^*}{m(1+cu^*)}$ and u^* can be solved from

$$\frac{rm(1+cu)}{m+(cm+kq)u} = d + au + \frac{pqu}{m(1+cu)^2}.$$

Denote $f(u) = \frac{rm(1+cu)}{m+(cm+kq)u}$ and $g(u) = d + au + \frac{pqu}{m(1+cu)^2}$. We can compute that

$$f(0) = r, \quad f'(u) = \frac{-mrkq}{(m+(cm+kq)u)^2} < 0 \quad \text{and} \quad \lim_{u \rightarrow \infty} f(u) = \frac{cmr}{cm+kq}$$

and

$$g(0) = d, \quad \lim_{u \rightarrow \infty} g(u) = \infty.$$

Thus, we conclude that if $r \leq d$, the curves of $f(u)$ and $g(u)$ do not intersect in the interval $(0, \infty)$ since $f(u)$ is decreasing and $g(u) > d$ for $u \in (0, \infty)$, and therefore model (4) has no positive equilibrium; while if $r > d$, the curves of $f(u)$ and $g(u)$ have at least one intersection point, which indicates that model (4) has at least one positive equilibrium (u^*, v^*) .

Now we perform the linear stability analysis of equilibria of model (4). The Jacobi matrix of model (4) is

$$J_{(u,v)} = \begin{pmatrix} \frac{r}{1+kv} - d - 2au - \frac{pv}{(1+cu)^2} & -\left(\frac{kru}{(1+kv)^2} + \frac{pu}{1+cu}\right) \\ \frac{qv}{(1+cu)^2} & \frac{qu}{1+cu} - 2mv \end{pmatrix}. \tag{5}$$

At the trivial equilibrium $(0, 0)$, the Jacobi matrix (5) has two two eigenvalues 0 and $r - d$. Thus, if $r > d$, $(0, 0)$ is unstable; if $r \leq d$, noticing that $u = 0$ and $v = 0$ are both the solutions of model (4) and there are no other equilibria in the positive quadrant, it then follows from the theory of Poincaré-Bendixson, the existence and uniqueness as well as the boundedness of solutions of model (4) that $(0, 0)$ is globally attractive in \mathbb{R}_+^2 . At the semi-trivial equilibrium $(\frac{r-d}{a}, 0)$, the two eigenvalues of (5) are $\lambda_1 = \frac{q(r-d)}{a+c(r-d)} > 0$ and $\lambda_2 = -(r-d) < 0$. Thus, $(\frac{r-d}{a}, 0)$ is always an unstable saddle.

At the positive equilibrium (u^*, v^*) , the corresponding characteristic equation is

$$\lambda^2 - (a_{11} + a_{22})\lambda + (a_{11}a_{22} - a_{12}a_{21}) = 0,$$

where

$$\begin{aligned} a_{11} &= \frac{r}{1+kv^*} - d - 2au^* - \frac{pv^*}{(1+cu^*)^2}, & a_{12} &= -\left(\frac{kru^*}{(1+kv^*)^2} + \frac{pu^*}{1+cu^*}\right), \\ a_{21} &= \frac{qv^*}{(1+cu^*)^2}, & a_{22} &= \frac{qu^*}{1+cu^*} - 2mv^*. \end{aligned}$$

Thus, (u^*, v^*) is locally asymptotically stable provided

$$a_{11} + a_{22} < 0, \quad a_{11}a_{22} - a_{12}a_{21} > 0. \tag{6}$$

To summarize, we have the following theorem.

Theorem 1 *Model (4) always has a trivial equilibrium $(0, 0)$, which is a global attractor provided $r \leq d$. When $r > d$, $(0, 0)$ becomes unstable, and a semi-trivial equilibrium $(\frac{r-d}{a}, 0)$ emerges, which is always a saddle; meantime, the model exists at least one positive equilibrium (u^*, v^*) , which is locally asymptotically stable provided (6) is satisfied.*

Since we are interested in a physically positive equilibrium, in the next section, we will focus our main attention on the one satisfying (6), and explore the influence of memory-based diffusion coefficient, memory-based delay and pregnant delay on the spatiotemporal dynamics of model (3). For the sake of mathematical analysis, we always assume that $\Omega = [0, l\pi]$ in this paper.

4 Reaction-diffusion prey-predator model with delays

The linearized system of model (3) at the positive constant steady state (u^*, v^*) is:

$$\begin{cases} \frac{\partial u(x, t)}{\partial t} = d_1 \Delta u(x, t) + \alpha u^* \Delta v_{\tau_1} + A_{11}u(x, t) + A_{12}v(x, t) + B_{12}v_{\tau_2}, & x \in \Omega, t > 0, \\ \frac{\partial v(x, t)}{\partial t} = d_2 \Delta v(x, t) + A_{21}u(x, t) + A_{22}v(x, t), & x \in \Omega, t > 0, \\ \frac{\partial u(x, t)}{\partial v} = 0, \frac{\partial v(x, t)}{\partial v} = 0, & x \in \partial\Omega, t > 0, \\ u(x, t) = u_0(x) \geq 0, v(x, t) = v_0(x) \geq 0, & x \in \Omega, t \in (-\max\{\tau_1, \tau_2\}, 0], \end{cases} \tag{7}$$

where $A_{11} = a_{11}, A_{12} = -\frac{pu^*}{1+cu^*}, A_{21} = a_{21}, A_{22} = a_{22}, B_{12} = \frac{-kru^*}{(1+kv^*)^2}$. Obviously, $A_{12} + B_{12} = a_{12}$, and the stability condition (6) can be written as

$$A_{11} + A_{22} < 0, \quad A_{11}A_{22} - (A_{12} + B_{12})A_{21} > 0. \tag{8}$$

It is well known that the negative Laplace operator $-\Delta$ subject to zero Neumann boundary condition

$$\begin{cases} -\Delta \xi = \mu \xi, & x \in \Omega \\ \xi'(x) = 0, & x \in \partial\Omega \end{cases} \tag{9}$$

has eigenvalues $\mu_n = \frac{n^2}{l^2}$ ($n = 0, 1, 2, \dots$) with $0 = \mu_0 < \mu_1 \leq \mu_2 \leq \dots \leq \mu_n \leq \dots$ and $\lim_{n \rightarrow \infty} \mu_n = \infty$ and the corresponding eigenfunctions $\xi_n(x) = \cos \frac{n}{l}x$. Let in (7) $u(x, t) = Ue^{\lambda t} \cos \frac{n}{l}x, v(x, t) = Ve^{\lambda t} \cos \frac{n}{l}x$. The characteristic equation of model (3) at (u^*, v^*) has the form

$$\Delta_n(\lambda, \tau_1, \tau_2, \alpha) := \lambda^2 + A_n\lambda + B_n + C_n e^{-\lambda\tau_1} + D e^{-\lambda\tau_2} = 0, \tag{10}$$

where

$$\begin{aligned}
 A_n &= (d_1 + d_2) \frac{n^2}{l^2} - (A_{11} + A_{22}), \\
 B_n &= \left(d_1 \frac{n^2}{l^2} - A_{11} \right) \left(d_2 \frac{n^2}{l^2} - A_{22} \right) - A_{12} A_{21}, \\
 C_n &= A_{21} \alpha u^* \frac{n^2}{l^2}, \quad D = -A_{21} B_{12}.
 \end{aligned}
 \tag{11}$$

The stability of (u^*, v^*) changes only when a root λ of (10) appears on and crosses the imaginary axis. To this end, assume that the eigenvalue λ has the form of $i\omega$ ($\omega \geq 0$). Then we have

$$\begin{aligned}
 -\omega^2 + B_n + C_n \cos(\omega\tau_1) + D \cos(\omega\tau_2) \\
 + i(A_n\omega - C_n \sin(\omega\tau_1) - D \sin(\omega\tau_2)) = 0.
 \end{aligned}
 \tag{12}$$

Depending on the values of ω and n , four kinds of solutions may be bifurcated from (u^*, v^*) : spatially homogeneous steady state solutions, nonconstant steady state solutions, spatially homogeneous periodic solutions and spatially nonhomogeneous periodic solutions.

Notice that when $\omega = 0$ and $n = 0$, spatially homogeneous steady state bifurcation may occur and the bifurcated solution should also be a constant steady state. In this situation, equation (12) becomes $B_0 + D = 0$, that is

$$A_{11}A_{22} - (A_{12} + B_{12})A_{21} = 0,$$

which is in contradiction with the second condition in (8). Therefore, this kind of bifurcation cannot occur.

4.1 Spatially homogeneous Hopf bifurcations

When $n = 0$ and $\omega \neq 0$, spatially homogeneous periodic solutions may emerge. Note that when $n = 0$, equation (12) becomes

$$-\omega^2 + B_0 + D \cos(\omega\tau_2) + i(A_0\omega - D \sin(\omega\tau_2)) = 0,
 \tag{13}$$

which contains only pregnancy delay τ_2 . This indicates that the spatially homogeneous periodic solutions cannot be bifurcated from (u^*, v^*) for model (3) with only spatial memory τ_1 . Therefore, in this subsection, we need only to consider the situation when $\tau_1 = 0$ and $\tau_2 > 0$. From (13) we can obtain that

$$\sin(\omega\tau_2) = \frac{A_0\omega}{D} > 0, \quad \cos(\omega\tau_2) = \frac{\omega^2 - B_0}{D},$$

and

$$\omega^4 + (A_0^2 - 2B_0)\omega^2 + B_0^2 - D^2 = 0. \tag{14}$$

Notice that $B_0^2 - D^2$ has the same sign as $B_0 - D$ since $B_0 + D > 0$. We treat (14) as a quadratic equation of ω^2 and consider the following three cases.

Case 1. $B_0 < D$

In this case, (14) has a unique positive root and then (10) has a pair of purely imaginary roots $\pm\omega_{2,0}^+i$, where

$$\omega_{2,0}^{+2} = \frac{-(A_0^2 - 2B_0) + \sqrt{A_0^4 - 4B_0A_0^2 + 4D^2}}{2}. \tag{15}$$

The corresponding critical values of delay τ_2 are

$$\tau_{2,0}^{j+} = \frac{1}{\omega_{2,0}^+} \left(\arccos \frac{\omega_{2,0}^{+2} - B_0}{D} + 2j\pi \right), \quad j = 0, 1, 2, \dots \tag{16}$$

As for the transversality condition, we claim that

$$\left. \frac{d\Re(\lambda)}{d\tau_2} \right|_{\tau_2=\tau_{2,0}^{j+}} > 0. \tag{17}$$

In fact, let $n = \tau_1 = 0$ in (10) and regard λ as a function of τ_2 . Taking the derivative with respect to τ_2 on both sides of (10), we obtain that

$$\left(\frac{d\Re(\lambda)}{d\tau_2} \right)^{-1} \Big|_{\tau_2=\tau_{2,0}^{j+}} = \frac{2\omega_{2,0}^{+2} + A_0^2 - 2B_0}{D^2} = \frac{\sqrt{A_0^4 - 4B_0A_0^2 + 4D^2}}{D^2} > 0. \tag{18}$$

Notice that the critical delay sequence $\{\tau_{2,0}^{j+}\}_{j=0}^\infty$ is increasing with respect to j . It then follows from (17) that if $\tau_2 = \tau_{2,0}^{j+}$, (10) has a pair of purely imaginary roots; if $0 < \tau_2 < \tau_{2,0}^{0+}$, all the roots of (10) have negative real parts, and if $\tau_2 > \tau_{2,0}^{0+}$, (10) has at least a pair of conjugate complex roots with positive real parts.

Case 2. $B_0 > D$ and $A_0^2 < 2(B_0 - \sqrt{B_0^2 - D^2})$.

In this case, (14) has two different positive roots and then (10) has two pairs of purely imaginary roots $\pm\omega_{2,0}^\pm i$, where

$$\omega_{2,0}^{\pm 2} = \frac{-(A_0^2 - 2B_0) \pm \sqrt{A_0^4 - 4B_0A_0^2 + 4D^2}}{2}. \tag{19}$$

The corresponding critical values of delay τ_2 are respectively

$$\tau_{2,0}^{j\pm} = \frac{1}{\omega_{2,0}^{\pm}} \left(\arccos \frac{\omega_{2,0}^{\pm 2} - B_0}{D} + 2j\pi \right), \quad j = 0, 1, 2, \dots \tag{20}$$

It is easy to know that the spacing between critical delay values in the subsequence $\{\tau_{2,0}^{j+}\}_{j=0}^\infty$ is $\frac{2\pi}{\omega_{2,0}^+}$ and that in the subsequence $\{\tau_{2,0}^{j-}\}_{j=0}^\infty$ is $\frac{2\pi}{\omega_{2,0}^-}$. Moreover, we can compute that for $j = 0, 1, 2, \dots$,

$$\begin{aligned} \left(\frac{d\Re(\lambda)}{d\tau_2} \right)^{-1} \Big|_{\tau_2=\tau_{2,0}^{j+}} &= \frac{1}{D^2} \sqrt{A_0^4 - 4B_0A_0^2 + 4D^2} > 0, \\ \left(\frac{d\Re(\lambda)}{d\tau_2} \right)^{-1} \Big|_{\tau_2=\tau_{2,0}^{j-}} &= -\frac{1}{D^2} \sqrt{A_0^4 - 4B_0A_0^2 + 4D^2} < 0. \end{aligned} \tag{21}$$

It follows that the positive jumps of the real part of the eigenvalues as τ_2 increases are more frequent than the negative jumps due to $\omega_{2,0}^+ > \omega_{2,0}^-$. Therefore, there is a $\kappa \geq 0$ such that when

$$\tau_2 \in (0, \tau_{2,0}^{0+}) \cup (\tau_{2,0}^{0-}, \tau_{2,0}^{1+}) \cup \dots \cup (\tau_{2,0}^{(\kappa-1)-}, \tau_{2,0}^{\kappa+}),$$

all the roots of (10) have negative real parts; when $\tau_2 = \tau_{2,0}^{j+}, j = 0, 1, 2, \dots, \kappa$ (resp. $\tau_2 = \tau_{2,0}^{j-}, j = 0, 1, 2, \dots, \kappa - 1$), all roots of (10) except $\pm i\omega_{2,0}^+$ (resp. $\pm i\omega_{2,0}^-$) have negative real parts; when

$$\tau_2 \in (\tau_{2,0}^{0+}, \tau_{2,0}^{0-}) \cup (\tau_{2,0}^{1+}, \tau_{2,0}^{1-}) \cup \dots \cup (\tau_{2,0}^{(\kappa-1)+}, \tau_{2,0}^{(\kappa-1)-}) \cup (\tau_{2,0}^{\kappa+}, +\infty),$$

(10) has at least a pair of conjugate complex roots with positive real parts.

Case 3. $B_0 > D$ and $A_0^2 > 2(B_0 - \sqrt{B_0^2 - D^2})$

In this case, (14) has no positive real roots, and therefore no Hopf bifurcations occur.

To summarize, we have the following lemma.

Lemma 1 Assume $r > d$ and (8) hold. For $\tau_1 = 0$ and $n = 0$, the following statements are true.

- (1) If $B_0 < D$, then (u^*, v^*) is asymptotically stable for $\tau_2 < \tau_{2,0}^{0+}$ and unstable for $\tau_2 > \tau_{2,0}^{0+}$. When $\tau_2 = \tau_{2,0}^{j+} (j = 0, 1, 2, \dots)$, model (3) undergoes a spatially homogeneous Hopf bifurcation at (u^*, v^*) .
- (2) If $B_0 > D$ and $A_0^2 < 2(B_0 - \sqrt{B_0^2 - D^2})$, then there is a $\kappa \geq 0$ such that (u^*, v^*) is asymptotically stable for $\tau_2 \in (0, \tau_{2,0}^{0+}) \cup \dots \cup (\tau_{2,0}^{(\kappa-1)-}, \tau_{2,0}^{\kappa+})$ and unstable for $\tau_2 \in (\tau_{2,0}^{0+}, \tau_{2,0}^{0-}) \cup \dots \cup (\tau_{2,0}^{\kappa+}, +\infty)$. When $\tau_2 = \tau_{2,0}^{j\pm} (j = 0, 1, 2, \dots)$, model (3) undergoes a spatially homogeneous Hopf bifurcation at (u^*, v^*) .

(3) If $B_0 > D$ and $A_0^2 > 2(B_0 - \sqrt{B_0^2 - D^2})$, then (u^*, v^*) is always asymptotically stable for all $\tau_2 \geq 0$.

4.2 Spatially nonhomogeneous steady state bifurcation

When $\omega = 0$ and $n \neq 0$, spatially nonhomogeneous steady state bifurcation may occur and the bifurcating solutions should be nonconstant steady state solutions. In this case, equation (12) can be simplified as $B_n + C_n + D = 0$, that is

$$d_1 d_2 \frac{n^4}{l^4} - (A_{11} d_2 + A_{22} d_1 - \alpha A_{21} u^*) \frac{n^2}{l^2} + A_{11} A_{22} - A_{21} (A_{12} + B_{12}) = 0. \tag{22}$$

Notice that (22) contains only n . This indicates that the occurrence of spatially nonhomogeneous steady bifurcation has nothing to do with spatial memory τ_1 and pregnancy cycle τ_2 . Thus, in this subsection, we only need to consider the situation when $\tau_1 = \tau_2 = 0$.

Now we treat (22) as an equation with respect to α and regard n as a positive real number, then

$$\alpha(n^2) = - \frac{d_1 d_2 n^4 - (A_{11} d_2 + A_{22} d_1) l^2 n^2 + (A_{11} A_{22} - A_{21} (A_{12} + B_{12})) l^4}{A_{21} u^* l^2 n^2}. \tag{23}$$

It follows that $\alpha(n^2) > 0$ if and only if

$$A_{11} d_2 + A_{22} d_1 > 0, \tag{24}$$

and

$$(A_{11} d_2 - A_{22} d_1)^2 + 4 d_1 d_2 A_{21} (A_{12} + B_{12}) > 0. \tag{25}$$

In (23), by taking the derivative with respect to n^2 , we have

$$\alpha'(n^2) = - \frac{d_1 d_2 n^4 - (A_{11} A_{22} - A_{21} (A_{12} + B_{12})) l^4}{A_{21} u^* l^2 n^4},$$

which indicates that $\alpha'(n^2) > 0$ if $n^2 < n_*^2$, and $\alpha'(n^2) < 0$ if $n^2 > n_*^2$, where

$$n_*^2 = l^2 \sqrt{\frac{A_{11} A_{22} - A_{21} (A_{12} + B_{12})}{d_1 d_2}}.$$

Therefore, the function $\alpha(n^2)$ reaches its positive maximum value α^* at n_T^2 , i.e., $\alpha^* = \alpha(n_T^2)$, where

$$n_T = \begin{cases} [n_*], & \text{if } \alpha([n_*]^2) > \alpha(([n_*] + 1)^2), \\ [n_*] + 1, & \text{if } \alpha([n_*]^2) < \alpha(([n_*] + 1)^2). \end{cases} \tag{26}$$

Here $[\cdot]$ is the integer part function. Moreover, we can deduce that $\alpha^* > 0$ if and only if

$$(A_{11}d_2 - A_{22}d_1)^2 + 4d_1d_2A_{21}(A_{12} + B_{12}) > \frac{(d_1d_2)^2}{l^4}. \tag{27}$$

It then follows that when $\alpha > \alpha^*$, there is no positive integer n^2 satisfying equation (22); while when $\alpha < \alpha^*$, there is always a positive integer n^2 such that $B_n + C_n + D < 0$.

As for the transversality condition, firstly, we show that $\lambda = 0$ is a simple eigenvalue of (10) with $\tau_1 = \tau_2 = 0$. In fact,

$$\left. \frac{\partial \Delta_n(\lambda, 0, 0, \alpha)}{\partial \lambda} \right|_{\lambda=0} = A_n > 0. \tag{28}$$

In addition, we can obtain from (10) that

$$\left. \frac{d\lambda}{d\alpha} \right|_{\lambda=0} = -\frac{A_{21}u^* n^2}{A_n l^2} < 0. \tag{29}$$

As a summary, we have the following lemma.

Lemma 2 *Assume $r > d$ and (8) hold. For $\tau_1 = \tau_2 = 0$, if (24) and (27) are satisfied, then there exists a positive integer n_T , which is defined in (26), such that $\alpha^* = \alpha(n_T^2) > 0$. Moreover, if $\alpha > \alpha^*$, there is no Turing instability; if $\alpha < \alpha^*$, there is at least one $n \in \mathbb{N}$ such that $B_n + C_n + D < 0$, that is, Turing instability occurs.*

Remark 1 From an ecological point of view, this result reveals that (u^*, v^*) will retain its stability for fast memory-based diffusion, but it is easy to generate spatial patterns for slow memory-based diffusion, which implies that fast chemotaxis is conducive to homogenization.

In the sequel of this section, we always assume that $\alpha > \alpha^*$, that is no Turing instability occurs and the constant steady state (u^*, v^*) is stable for model (3) without delay.

4.3 Spatially nonhomogeneous Hopf bifurcations

When $\omega \neq 0$ and $n \neq 0$, spatially nonhomogeneous periodic solutions may emerge. In this case, we need only consider three scenarios when $\alpha > \alpha^*$: (i) $\tau_1 > 0, \tau_2 = 0$; (ii) $\tau_1 = 0, \tau_2 > 0$, and (iii) $\tau_1, \tau_2 > 0$.

4.3.1 $\tau_1 > 0, \tau_2 = 0$

In this scenario, equation (12) becomes

$$-\omega^2 + B_n + C_n \cos(\omega\tau_1) + D + i(A_n\omega - C_n \sin(\omega\tau_1)) = 0, \tag{30}$$

from which we obtain that

$$\sin(\omega\tau_1) = \frac{A_n\omega}{C_n} > 0, \quad \cos(\omega\tau_1) = \frac{\omega^2 - (B_n + D)}{C_n},$$

and

$$\omega^4 + (A_n^2 - 2(B_n + D))\omega^2 + (B_n + D)^2 - C_n^2 = 0. \tag{31}$$

Notice that $\alpha > \alpha^*$ implies that $(B_n + D)^2 - C_n^2 \neq 0$ for all $n \in \mathbb{N} \setminus \{0\}$. Regarding (31) as a quadratic equation of ω^2 , we consider the following three cases.

Case 1. There exists a $n \in \mathbb{N} \setminus \{0\}$ such that

$$(B_n + D)^2 - C_n^2 < 0. \tag{32}$$

In this case, (31) has a unique positive root, which implies that (10) has a pair of purely imaginary roots $\pm\omega_{1,n}^+ i$, where

$$\omega_{1,n}^{+2} = \frac{-(A_n^2 - 2(B_n + D)) + \sqrt{A_n^4 - 4(B_n + D)A_n^2 + 4C_n^2}}{2}, \tag{33}$$

and the corresponding critical values of τ_1 are

$$\tau_{1,n}^{j+} = \frac{1}{\omega_{1,n}^+} \left(\arccos \frac{\omega_{1,n}^{+2} - (B_n + D)}{C_n} + 2j\pi \right), \quad j = 0, 1, 2, \dots \tag{34}$$

Notice that for each fixed n satisfying (32), the critical delay sequence $\{\tau_{1,n}^{j+}\}_{j=0}^\infty$ is increasing with respect to j . For all n satisfying (32), denote

$$\tau_1^* := \tau_{1,n_c}^{0+} = \min_n \{\tau_{1,n}^{0+}\}, \tag{35}$$

where n_c is the n such that τ_{1,n_c}^{0+} is the minimum of the sequence $\{\tau_{1,n}^{0+}\}$. Obviously, τ_1^* is also the minimum value of the sequence $\{\tau_{1,n}^{j+}\}_{j=0}^\infty$. Moreover, we can compute that

$$\frac{d\Re(\lambda)}{d\tau_1} \Big|_{\tau_1=\tau_{1,n}^{j+}} = \frac{\sqrt{A_n^4 - 4(B_n + D)A_n^2 + 4C_n^2}}{C_n^2} > 0.$$

It then follows that when $0 < \tau_1 < \tau_1^*$, all the roots of (10) have negative real parts; when $\tau_1 = \tau_1^*$, all the roots of (10) except $\pm i\omega_{1,n}^+$ have negative real parts; when $\tau_1 > \tau_1^*$, (10) has at least a pair of conjugate complex roots with positive real parts.

Case 2. There exists a $n \in \mathbb{N} \setminus \{0\}$ such that

$$(B_n + D)^2 - C_n^2 > 0, \quad A_n^2 < 2 \left((B_n + D) - \sqrt{(B_n + D)^2 - C_n^2} \right). \quad (36)$$

In this case, (31) has two distinct positive roots, which implies that (10) has two pairs of purely imaginary roots $\pm \omega_{1,n}^\pm i$, where

$$\omega_{1,n}^{\pm 2} = \frac{-(A_n^2 - 2(B_n + D)) \pm \sqrt{A_n^4 - 4(B_n + D)A_n^2 + 4C_n^2}}{2}. \quad (37)$$

Then the corresponding critical values of τ_1 are

$$\tau_{1,n}^{j\pm} = \frac{1}{\omega_{1,n}^\pm} \left(\arccos \frac{\omega_{1,n}^{\pm 2} - (B_n + D)}{C_n} + 2j\pi \right), \quad j = 0, 1, 2, \dots \quad (38)$$

Moreover, we can compute that for $j = 0, 1, 2, \dots$,

$$\begin{aligned} \left. \frac{d\Re(\lambda)}{d\tau_1} \right|_{\tau_1=\tau_{1,n}^{j+}} &= \frac{1}{C_n^2} \sqrt{A_n^4 - 4(B_n + D)A_n^2 + 4C_n^2} > 0, \\ \left. \frac{d\Re(\lambda)}{d\tau_1} \right|_{\tau_1=\tau_{1,n}^{j-}} &= -\frac{1}{C_n^2} \sqrt{A_n^4 - 4(B_n + D)A_n^2 + 4C_n^2} < 0. \end{aligned} \quad (39)$$

Thus, for each fixed $n \neq 0$ satisfying (36), both $\{\tau_{1,n}^{j+}\}_{j=0}^\infty$ and $\{\tau_{1,n}^{j-}\}_{j=0}^\infty$ are increasing with respect to j . Moreover, the spacing between critical delay values in the subsequence $\{\tau_{1,n}^{j+}\}_{j=0}^\infty$ is $\frac{2\pi}{\omega_{1,n}^+}$ and that in the subsequence $\{\tau_{1,n}^{j-}\}_{j=0}^\infty$ is $\frac{2\pi}{\omega_{1,n}^-}$. It follows from (39) that the positive jumps of the real part of the eigenvalues as τ_1 increases are more frequent than the negative jumps due to $\omega_{1,n}^+ > \omega_{1,n}^-$. Notice also that $\{\tau_{1,n}^{j+}\} < \{\tau_{1,n}^{j-}\}$ for all n . Define $\tau_1^* := \min_n \{\tau_{1,n}^{0+}\}$. Then τ_1^* is minimum critical value of delay τ_1 . For the convenience of narration, for all $n \neq 0$ satisfying (36), we reorder the delay subsequence $\{\tau_{1,n}^{j+}\}_{j=0}^\infty$ (resp. $\{\tau_{1,n}^{j-}\}_{j=0}^\infty$) as an increasing order and denote the resulting sequence as $\{\tau_1^{s+}\}_{s=1}^\infty$ (resp. $\{\tau_1^{s-}\}_{s=1}^\infty$). Notice that $\tau_1^* = \tau_1^{0+}$. Therefore, there must have a $\kappa_1 \geq 0$ such that when

$$\tau_1 \in (0, \tau_1^{0+}) \cup (\tau_1^{0-}, \tau_1^{1+}) \cup \dots \cup (\tau_1^{(\kappa_1-1)-}, \tau_1^{\kappa_1+}),$$

all the roots of (10) have negative real parts; when

$$\tau_1 \in (\tau_1^{0+}, \tau_1^{0-}) \cup (\tau_1^{1+}, \tau_1^{1-}) \cup \dots \cup (\tau_1^{(\kappa_1-1)+}, \tau_1^{(\kappa_1-1)-}) \cup (\tau_1^{\kappa_1+}, +\infty),$$

(10) has at least a pair of conjugate complex roots with positive real parts.

Case 3. For any $n \in \mathbb{N} \setminus \{0\}$,

$$(B_n + D)^2 - C_n^2 > 0, \quad A_n^2 > 2 \left((B_n + D) - \sqrt{(B_n + D)^2 - C_n^2} \right). \quad (40)$$

In this case, there is nothing to say.

To summarize, we have the following lemma.

Lemma 3 Assume $r > d, \alpha > \alpha^*$ and (8) hold. For $\tau_2 = 0$ and $n \neq 0$, the following statements are true.

- (1) If there exists a $n \in \mathbb{N} \setminus \{0\}$ such that (32) holds, then (u^*, v^*) is asymptotically stable for $\tau_1 < \tau_1^* = \min_n \{\tau_{1,n}^{0+}\}$ and unstable for $\tau_1 > \tau_1^*$. When $\tau_1 = \tau_{1,n}^{j+}$ ($j = 0, 1, 2, \dots$), model (3) undergoes a spatially nonhomogeneous Hopf bifurcation at (u^*, v^*) .
- (2) If there exists a $n \in \mathbb{N} \setminus \{0\}$ such that (36) holds, then there is a $\kappa_1 \geq 0$ and a sequence $\{\tau_1^{s\pm}\}_{s=0}^\infty$ such that (u^*, v^*) is asymptotically stable for $\tau_1 \in (0, \tau_1^{0+}) \cup \dots \cup (\tau_1^{(\kappa_1-1)-}, \tau_1^{\kappa_1+})$ and unstable for $\tau_1 \in (\tau_1^{0+}, \tau_1^{0-}) \cup \dots \cup (\tau_1^{\kappa_1+}, +\infty)$. When $\tau_1 = \tau_1^{s\pm}$ ($s = 0, 1, 2, \dots$), model (3) undergoes a spatially nonhomogeneous Hopf bifurcation at (u^*, v^*) .
- (3) If (40) is satisfied for all $n \in \mathbb{N} \setminus \{0\}$, then (u^*, v^*) is always asymptotically stable for all $\tau_1 \geq 0$.

4.3.2 $\tau_1 = 0, \tau_2 > 0$

Arguing similarly as in the scenario when $\tau_1 > 0$ and $\tau_2 = 0$, we can obtain the corresponding results. To avoid repetition, we just provide the results as a lemma. Denote

$$\omega_{2,n}^{\pm 2} = \frac{-(A_n^2 - 2(B_n + C_n)) \pm \sqrt{A_n^4 - 4(B_n + C_n)A_n^2 + 4D^2}}{2}, \quad (41)$$

$$\tau_{2,n}^{j\pm} = \frac{1}{\omega_{2,n}^\pm} \left(\arccos \frac{\omega_{2,n}^{\pm 2} - (B_n + C_n)}{D} + 2j\pi \right), \quad j = 0, 1, 2, \dots, \quad (42)$$

$$\tau_2^* = \min_{n \in \mathbb{N} \setminus \{0\}} \{\tau_{2,n}^{0+}\}. \quad (43)$$

Lemma 4 Assume $r > d, \alpha > \alpha^*$ and (8) hold. For $\tau_1 = 0$ and $n \neq 0$, the following statements are true.

- (1) If there exists a $n \in \mathbb{N} \setminus \{0\}$ such that $(B_n + C_n)^2 - D^2 < 0$, then (u^*, v^*) is asymptotically stable for $\tau_2 < \tau_2^*$ and unstable for $\tau_2 > \tau_2^*$. When $\tau_2 = \tau_{2,n}^{j+}$ ($j =$

- 0, 1, 2, ...), model (3) undergoes a spatially nonhomogeneous Hopf bifurcation at (u^*, v^*) .
- (2) If there exists a $n \in \mathbb{N} \setminus \{0\}$ such that $(B_n + C_n)^2 - D^2 > 0$ and $A_n^2 < 2((B_n + C_n) - \sqrt{(B_n + C_n)^2 - D^2})$, then there is a $\kappa_2 \geq 0$ and an increasing sequence $\{\tau_2^{s\pm}\}_{s=0}^\infty$ such that (u^*, v^*) is asymptotically stable for $\tau_2 \in (0, \tau_2^{0+}) \cup \dots \cup (\tau_2^{(\kappa_2-1)-}, \tau_2^{\kappa_2+})$ and unstable for $\tau_2 \in (\tau_2^{0+}, \tau_2^{0-}) \cup \dots \cup (\tau_2^{\kappa_2+}, +\infty)$. When $\tau_2 = \tau_2^{s\pm}$ ($s = 0, 1, 2, \dots$), model (3) undergoes a spatially nonhomogeneous Hopf bifurcation at (u^*, v^*) .
- (3) If $(B_n + C_n)^2 - D^2 > 0$ and $A_n^2 > 2((B_n + C_n) - \sqrt{(B_n + C_n)^2 - D^2})$ for all $n \in \mathbb{N} \setminus \{0\}$, then (u^*, v^*) is always asymptotically stable for all $\tau_2 \geq 0$.

4.3.3 $\tau_1, \tau_2 > 0$

We have analyzed the two scenarios when model (3) has only a single delay above. Then, how does the Hopf bifurcation behave when the two time delays both exist? We will use the geometric method proposed in Gu et al. (2005) to discuss this issue. Also, we assume that $\alpha > \alpha^*$, i.e., the positive equilibrium (u^*, v^*) is linearly stable for model (3) with $\tau_1 = \tau_2 = 0$.

For this purpose, we rewrite the characteristic equation (10) as

$$D_n(\lambda, \tau_1, \tau_2) := P_{0,n}(\lambda) + P_{1,n}(\lambda)e^{-\lambda\tau_1} + P_{2,n}(\lambda)e^{-\lambda\tau_2} = 0, \tag{44}$$

where

$$P_{0,n}(\lambda) = \lambda^2 + A_n\lambda + B_n, \quad P_{1,n}(\lambda) = C_n, \quad P_{2,n}(\lambda) = D, \tag{45}$$

where A_n, B_n, C_n and D are defined in (11). Obviously, for each n , $P_{0,n}(\lambda), P_{1,n}(\lambda)$ and $P_{2,n}(\lambda)$ satisfy the assumptions (I)–(IV) in Gu et al. (2005). Denote

$$a_1^n(\lambda) = \frac{P_{1,n}(\lambda)}{P_{0,n}(\lambda)}, \quad a_2^n(\lambda) = \frac{P_{2,n}(\lambda)}{P_{0,n}(\lambda)}. \tag{46}$$

Then the characteristic equation (44) becomes

$$a^n(\lambda; \tau_1, \tau_2) := 1 + a_1^n(\lambda)e^{-\lambda\tau_1} + a_2^n(\lambda)e^{-\lambda\tau_2} = 0. \tag{47}$$

As argued above, when the equilibrium loses its stability, there is at least one characteristic root λ that appears on and crosses the imaginary axis from left to right. Notice that 0 is not a root of (47). Therefore, we only need to determine the conditions that $\lambda = i\omega$ ($\omega > 0$) satisfies (47). Notice also that $P_{s,n}(i\omega) \neq 0$ ($s = 0, 1, 2$) for all $\omega > 0$. By Proposition 3.1 in Gu et al. (2005), we know that $\lambda = i\omega$ ($\omega > 0$) is a solution of (47) if and only if the set

$$\Omega_n = \{\omega \in \mathbb{R}_+ : |a_1^n(i\omega)| + |a_2^n(i\omega)| \geq 1, \quad -1 \leq |a_1^n(i\omega)| - |a_2^n(i\omega)| \leq 1\}. \tag{48}$$

is nonempty. Ω_n is called the crossing set and consists of a finite number of intervals with finite length (Gu et al. 2005). Obviously, if we assume these intervals as $\Omega_{n,k}$, $k = 1, 2, \dots, N$ and they are arranged by the way that the left end of $\Omega_{n,k}$ is increasing with respect to k , then $\Omega_n = \bigcup_{k=1}^N \Omega_{n,k}$. The following lemma is about the basic form of the crossing set Ω_n .

Lemma 5 For any $n \in \mathbb{N} \setminus \{0\}$,

(1) When $C_n + D < |B_n|$,

(1a) If $A_n^2 > 2(B_n - \sqrt{B_n^2 - (C_n + D)^2})$, then $\Omega_n = \emptyset$;

(1b) If $2(B_n - \sqrt{B_n^2 - (C_n - D)^2}) \leq A_n^2 < 2(B_n - \sqrt{B_n^2 - (C_n + D)^2})$, then

$$\Omega_n = [\omega_n^{1,l}, \omega_n^{1,r}]; \tag{49}$$

(1c) If $A_n^2 < 2(B_n - \sqrt{B_n^2 - (C_n - D)^2})$, then

$$\Omega_n = \Omega_{n,1} \cup \Omega_{n,2} = [\omega_n^{1,l}, \omega_n^{2,l}] \cup [\omega_n^{2,r}, \omega_n^{1,r}]. \tag{50}$$

(2) When $C_n + D > |B_n|$,

(2a) If $|C_n - D| < |B_n|$, $A_n^2 \geq 2(B_n - \sqrt{B_n^2 - (C_n - D)^2})$, then

$$\Omega_n = (0, \omega_n^{1,r}]; \tag{51}$$

(2b) If $|C_n - D| < |B_n|$, $A_n^2 < 2(B_n - \sqrt{B_n^2 - (C_n - D)^2})$, then

$$\Omega_n = \Omega_{n,1} \cup \Omega_{n,2} = (0, \omega_n^{2,l}] \cup [\omega_n^{2,r}, \omega_n^{1,r}]; \tag{52}$$

(2c) If $|C_n - D| > |B_n|$, then

$$\Omega_n = [\omega_n^{2,r}, \omega_n^{1,r}]. \tag{53}$$

Here

$$\begin{aligned} \omega_n^{1,l} &= \sqrt{\frac{-(A_n^2 - 2B_n) - \sqrt{\Delta_1}}{2}}, & \omega_n^{1,r} &= \sqrt{\frac{-(A_n^2 - 2B_n) + \sqrt{\Delta_1}}{2}}, \\ \omega_n^{2,l} &= \sqrt{\frac{-(A_n^2 - 2B_n) - \sqrt{\Delta_2}}{2}}, & \omega_n^{2,r} &= \sqrt{\frac{-(A_n^2 - 2B_n) + \sqrt{\Delta_2}}{2}}, \end{aligned}$$

and

$$\begin{aligned} \Delta_1 &= A_n^4 - 4B_n A_n^2 + 4(C_n + D)^2, \\ \Delta_2 &= A_n^4 - 4B_n A_n^2 + 4(C_n - D)^2. \end{aligned} \tag{54}$$

Proof From (45) and (46), we can obtain that

$$1 = |a_1^n(i\omega)| + |a_2^n(i\omega)| = \frac{C_n + D}{\sqrt{(-\omega^2 + B_n)^2 + A_n^2\omega^2}}, \tag{55}$$

which is equivalent to

$$\omega^4 + (A_n^2 - 2B_n)\omega^2 + B_n^2 - (C_n + D)^2 = 0. \tag{56}$$

We can easily check that

- when $C_n + D < |B_n|$, if $A_n^2 > 2(B_n - \sqrt{B_n^2 - (C_n + D)^2})$, then $|a_1^n(i\omega)| + |a_2^n(i\omega)| < 1$ for all $\omega > 0$, which violates the first condition of (48), and therefore, $\Omega_n = \emptyset$; if $A_n^2 < 2(B_n - \sqrt{B_n^2 - (C_n + D)^2})$, then $|a_1^n(i\omega)| + |a_2^n(i\omega)| \geq 1$ for $\omega \in [\omega_n^{1,l}, \omega_n^{1,r}]$;
- when $C_n + D > |B_n|$, then $|a_1^n(i\omega)| + |a_2^n(i\omega)| \geq 1$ for all $\omega \in (0, \omega_n^{1,r}]$.

On the other hand, $||a_1^n(i\omega)| - |a_2^n(i\omega)|| = 1$ is equivalent to

$$\omega^4 + (A_n^2 - 2B_n)\omega^2 + B_n^2 - (C_n - D)^2 = 0. \tag{57}$$

Similarly, we can also have

- when $|C_n - D| < |B_n|$, if $A_n^2 \geq 2(B_n - \sqrt{B_n^2 - (C_n - D)^2})$, then $-1 \leq |a_1^n(i\omega)| - |a_2^n(i\omega)| \leq 1$ for all $\omega \in (0, \infty)$; if $A_n^2 < 2(B_n - \sqrt{B_n^2 - (C_n - D)^2})$, then $-1 \leq |a_1^n(i\omega)| - |a_2^n(i\omega)| \leq 1$ for all $\omega \in (0, \omega_n^{2,l}] \cup [\omega_n^{2,r}, +\infty)$;
- When $|C_n - D| > |B_n|$, then $-1 \leq |a_1^n(i\omega)| - |a_2^n(i\omega)| \leq 1$ for all $\omega \in [\omega_n^{2,r}, +\infty)$.

In addition, from (54), we can see that $\Delta_1 > \Delta_2$, which implies that $\omega_n^{1,l} < \omega_n^{2,l}$ and $\omega_n^{2,r} < \omega_n^{1,r}$. To summarize, we can obtain the results on Ω_n listed in Lemma 5. \square

Remark 2 It is easy to see that $B_n - (C_n + D) \rightarrow \infty$ and $A_n^2 - 2(B_n - \sqrt{B_n^2 - (C_n + D)^2}) \rightarrow \infty$ as $n \rightarrow \infty$. Then from Lemma 5 (1a) we know that $\Omega_n = \emptyset$ for n large enough such that the following conditions hold:

$$C_n + D < |B_n|, A_n^2 > 2(B_n - \sqrt{B_n^2 - (C_n + D)^2}). \tag{58}$$

If Ω_n is nonempty, then for any $\omega \in \Omega_n$, one can express the pairs of time delays (τ_1, τ_2) satisfying (48) as

$$\tau_{1,n,k_1}^\pm(\omega) = \frac{\phi_{1,n}(\omega) + (2k_1 - 1)\pi \pm \psi_{1,n}(\omega)}{\omega}, k_1 = k_{1,n}^\pm, k_{1,n}^\pm + 1, k_{1,n}^\pm + 2, \dots, \tag{59}$$

$$\tau_{2,n,k_2}^\pm(\omega) = \frac{\phi_{2,n}(\omega) + (2k_2 - 1)\pi \mp \psi_{2,n}(\omega)}{\omega}, k_2 = k_{2,n}^\pm, k_{2,n}^\pm + 1, k_{2,n}^\pm + 2, \dots, \tag{60}$$

where

$$\begin{aligned} \psi_{1,n}(\omega) &= \arccos\left(\frac{1 + |a_1^n(i\omega)| + |a_2^n(i\omega)|}{2|a_1^n(i\omega)|}\right), \\ \psi_{2,n}(\omega) &= \arccos\left(\frac{1 + |a_1^n(i\omega)| + |a_2^n(i\omega)|}{2|a_2^n(i\omega)|}\right), \end{aligned}$$

and $\phi_{1,n}(\omega)$ and $\phi_{2,n}(\omega)$ are respectively the arguments of $a_1^n(i\omega)$ and $a_2^n(i\omega)$. $k_{1,n}^+$, $k_{1,n}^-$, $k_{2,n}^+$ and $k_{2,n}^-$ are the smallest integers such that τ_{1,n,k_1}^+ , τ_{1,n,k_1}^- , τ_{2,n,k_2}^+ and τ_{2,n,k_2}^- are nonnegative. Then the mode- n stability switching curves of (44) can be expressed by

$$\mathcal{T}_n = \bigcup_{k=1}^N \mathcal{T}_n^k, \tag{61}$$

where

$$\mathcal{T}_n^k = \bigcup_{k_1=-\infty}^{+\infty} \bigcup_{k_2=-\infty}^{+\infty} (\mathcal{T}_{n,k_1,k_2}^{+k}, \mathcal{T}_{n,k_1,k_2}^{-k}) \cap \mathbb{R}_+^2, \tag{62}$$

$$\mathcal{T}_{n,k_1,k_2}^{\pm k} = \left\{ \left(\tau_{1,n,k_1}^{\pm}(\omega), \tau_{2,n,k_2}^{\mp}(\omega) \right) : \omega \in \Omega_{n,k} \right\}. \tag{63}$$

For given n , \mathcal{T}_n is the set of all the points (τ_1, τ_2) in \mathbb{R}_+^2 satisfying that $D_n(\lambda, \tau_1, \tau_2)$ has at least one root $i\omega$.

Now, we describe the geometric structures of stability switching curves \mathcal{T}_n . Firstly, we follow the notations in Gu et al. (2005) to introduce the following four types of the ends of $\Omega_{n,k}$: (0) Type 0, when the left end of $\Omega_{n,k}$ is 0; (1) Type 1, when the end of $\Omega_{n,k}$ satisfies $|a_1^n(i\omega)| - |a_2^n(i\omega)| = 1$; (2) Type 2, when the end of $\Omega_{n,k}$ satisfies $|a_2^n(i\omega)| - |a_1^n(i\omega)| = 1$; (3) Type 3, when the end of $\Omega_{n,k}$ satisfies $|a_1^n(i\omega)| + |a_2^n(i\omega)| = 1$. $\Omega_{n,k}$ is called as type lr if the left end of $\Omega_{n,k}$ is of type l and its right end is of type r . In this way, $\Omega_{n,k}$ appeared in Lemma 5 can then be classified as follows. If $\Omega_{n,k} = [\omega_n^{1,l}, \omega_n^{1,r}]$, then it is of type 33. If $\Omega_{n,k} = (0, \omega_n^{1,r}]$, then it is of type 03. When $C_n > D$, $\Omega_{n,k} = [\omega_n^{1,l}, \omega_n^{2,l}]$ is of type 31, $\Omega_{n,k} = [\omega_n^{2,r}, \omega_n^{1,r}]$ is of type 13, $\Omega_{n,k} = (0, \omega_n^{2,l}]$ is of type 01; while when $C_n < D$, $\Omega_{n,k} = [\omega_n^{1,l}, \omega_n^{2,l}]$ is of type 32, $\Omega_{n,k} = [\omega_n^{2,r}, \omega_n^{1,r}]$ is of type 23, $\Omega_{n,k} = (0, \omega_n^{2,l}]$ is of type 02.

Based on Proposition 4.5 in Gu et al. (2005), we can obtain the structures of the mode- n stability switching curves \mathcal{T}_n . From Remark 2, we know that \mathcal{T}_n is an empty set for large n satisfying (58). For other n , we have the following lemma.

Lemma 6 *The mode- n stability switching curves \mathcal{T}_n may have the following structures in τ_1 - τ_2 plane:*

- (1) When $C_n + D < |B_n|$,

(1a) \mathcal{T}_n is a series of closed curves if

$$2\left(B_n - \sqrt{B_n^2 - (C_n - D)^2}\right) \leq A_n^2 < 2\left(B_n - \sqrt{B_n^2 - (C_n + D)^2}\right). \quad (64)$$

(1b) \mathcal{T}_n is a series of spiral-like curves with axes oriented τ_2 -axis if

$$C_n - D > 0, A_n^2 < 2\left(B_n - \sqrt{B_n^2 - (C_n - D)^2}\right). \quad (65)$$

(1c) \mathcal{T}_n is a series of spiral-like curves with axes oriented τ_1 -axis if

$$C_n - D < 0, A_n^2 < 2\left(B_n - \sqrt{B_n^2 - (C_n - D)^2}\right). \quad (66)$$

(2) When $C_n + D > |B_n|$,

(2a) \mathcal{T}_n is a series of open ended curves with both ends approaching infinity if

$$|C_n - D| < |B_n|, A_n^2 \geq 2\left(B_n - \sqrt{B_n^2 - (C_n - D)^2}\right). \quad (67)$$

(2b) \mathcal{T}_n consists of two kinds of curves: one is a series of open ended curves with both ends approaching infinity, and the other one is a series of spiral-like curves with axes oriented τ_2 -axis if

$$0 < C_n - D < |B_n|, A_n^2 < 2\left(B_n - \sqrt{B_n^2 - (C_n - D)^2}\right). \quad (68)$$

(2c) \mathcal{T}_n consists of two kinds of curves: one is a series of open ended curves with both ends approaching infinity, and the other one is a series of spiral-like curves with axes oriented τ_1 -axis if

$$-|B_n| < C_n - D < 0, A_n^2 < 2\left(B_n - \sqrt{B_n^2 - (C_n - D)^2}\right). \quad (69)$$

(2d) \mathcal{T}_n is a series of spiral-like curves with axes oriented τ_2 -axis if

$$C_n - D > |B_n|. \quad (70)$$

(2e) \mathcal{T}_n is a series of spiral-like curves with axes oriented τ_1 -axis if

$$C_n - D < -|B_n|. \quad (71)$$

Remark 3 In fact, $C_n > D$ implies that $\alpha > \frac{-B_1 2l^2}{u^* n^2}$. This indicates that if n is fixed, then for fast memory-based diffusion, the mode- n stability switching curves \mathcal{T}_n is a series of spiral-like curves with axes oriented τ_2 -axis; while for slow memory-based diffusion, \mathcal{T}_n is a series of spiral-like curves with axes oriented τ_1 -axis.

In the following paragraphs, we investigate the crossing direction of the roots of (44) when they cross the imaginary axis. For any stability switching curves $\mathcal{T}_{n,k_1,k_2}^{\pm k}$, we refer to the direction in which ω increases as the positive direction of the curves. We also refer to the region on the left-hand side as the region on the left when we go forward in the positive direction of the curve. Similarly, the right region can be defined suitably.

Let $\lambda = \sigma + i\omega$, then the implicit function theorem indicates that τ_1, τ_2 can be expressed as a function of σ and ω . From (47), we can compute that

$$\begin{aligned}
 R_1 &= -\Re\left(\frac{1}{\lambda} \frac{\partial a^n(\lambda; \tau_1, \tau_2)}{\partial \tau_1}\right)\Bigg|_{\lambda=i\omega} \\
 &= \frac{C_n}{\omega^4 + (A_n^2 - 2B_n)\omega^2 + B_n^2} \left((-\omega^2 + B_n) \cos(\omega\tau_1) - A_n\omega \sin(\omega\tau_1) \right), \\
 I_1 &= -\Im\left(\frac{1}{\lambda} \frac{\partial a^n(\lambda; \tau_1, \tau_2)}{\partial \tau_1}\right)\Bigg|_{\lambda=i\omega} \\
 &= \frac{-C_n}{\omega^4 + (A_n^2 - 2B_n)\omega^2 + B_n^2} \left((-\omega^2 + B_n) \sin(\omega\tau_1) + A_n\omega \cos(\omega\tau_1) \right), \\
 R_2 &= -\Re\left(\frac{1}{\lambda} \frac{\partial a^n(\lambda; \tau_1, \tau_2)}{\partial \tau_2}\right)\Bigg|_{\lambda=i\omega} \\
 &= \frac{D}{\omega^4 + (A_n^2 - 2B_n)\omega^2 + B_n^2} \left((-\omega^2 + B_n) \cos(\omega\tau_2) - A_n\omega \sin(\omega\tau_2) \right), \\
 I_2 &= -\Im\left(\frac{1}{\lambda} \frac{\partial a^n(\lambda; \tau_1, \tau_2)}{\partial \tau_2}\right)\Bigg|_{\lambda=i\omega} \\
 &= \frac{-D}{\omega^4 + (A_n^2 - 2B_n)\omega^2 + B_n^2} \left((-\omega^2 + B_n) \sin(\omega\tau_2) + A_n\omega \cos(\omega\tau_2) \right).
 \end{aligned}$$

It follows that

$$R_2 I_1 - R_1 I_2 = \frac{-C_n D}{\omega^4 + (A_n^2 - 2B_n)\omega^2 + B_n^2} \sin(\omega(\tau_1 - \tau_2)), \tag{72}$$

which is positive provided

$$\sin(\omega(\tau_1 - \tau_2)) < 0, \tag{73}$$

due to the fact that the denominator $\omega^4 + (A_n^2 - 2B_n)\omega^2 + B_n^2 > 0$ for all $\omega > 0$. By Proposition 6.1 in Gu et al. (2005), we arrive at the following conclusion.

Lemma 7 *Let $\omega \in \Omega_{n,k}$ and $(\tau_1, \tau_2) \in \mathcal{T}_{n,k_1,k_2}^{\pm k}$ such that $\lambda = i\omega$ is a simple root of $a^n(\lambda; \tau_1, \tau_2) = 0$. Then as (τ_1, τ_2) moves from the region on the right to the region on the left of the stability switching curve, a pair of conjugate complex roots of (47) cross the imaginary axis to the right if (73) is satisfied and if (73) is reversed, the crossing is in the opposite direction.*

Now, according to Lemmas 1, 2, 6 and 7, we arrive at the following stability results of (u_*, v_*) .

Theorem 2 Assume that $r > d, \alpha > \alpha^*$, (8) hold. Then

- (1) If $B_0 > D, A_0^2 > 2(B_0 - \sqrt{B_0^2 - D^2})$ holds for $n = 0$ and (58) holds for each $n \in \mathbb{N} \setminus \{0\}$, then (u_*, v_*) is always stable for all $\tau_1, \tau_2 \geq 0$.
- (2) If either $B_0 < D$ or $B_0 > D, A_0^2 < 2(B_0 - \sqrt{B_0^2 - D^2})$ holds for $n = 0$ and (58) holds for each $n \in \mathbb{N} \setminus \{0\}$, then there exists a $\tau_2^* > 0$ such that (u_*, v_*) is stable for $\tau_1 \geq 0$ and $\tau_2 < \tau_2^*$.
- (3) If either $B_0 < D$ or $B_0 > D, A_0^2 < 2(B_0 - \sqrt{B_0^2 - D^2})$ holds for $n = 0$ and either $C_n + D > |B_n|$ or $C_n + D < |B_n|, A_n^2 < 2(B_n - \sqrt{B_n^2 - (C_n + D)^2})$ holds for some $n \in \mathbb{N} \setminus \{0\}$, then there exist some delay pairs (τ_1^0, τ_2^0) and ω^0 such that $i\omega^0$ is a simple root of the characteristic equation (47). Moreover, if $\omega^0(\tau_1^0 - \tau_2^0) \neq k\pi$ ($k \in \mathbb{Z}$), then there exists a neighborhood U of (τ_1^0, τ_2^0) such that (u_*, v_*) is linearly stable for $(\tau_1, \tau_2) \in U \cap \Theta$ and unstable for $(\tau_1, \tau_2) \in U \setminus \Theta$, where Θ is the stable region enclosed by τ_1 - and τ_2 -axis and all the stability switching curves $\bigcup_n \mathcal{T}_n$, but not including $\bigcup_n \mathcal{T}_n$.

Proof (1) From Lemma 1 we know that (u_*, v_*) is linearly stable for model (3) with $n = 0$ when $B_0 > D, A_0^2 > 2(B_0 - \sqrt{B_0^2 - D^2})$. In addition, we know from Lemma 6 that for each $n \in \mathbb{N} \setminus \{0\}$, if (58) holds, then $\bigcup_{n \neq 0} \mathcal{T}_n$ is an empty set. Therefore, we have that when $\alpha > \alpha^*$, (u_*, v_*) is always stable for any $\tau_1, \tau_2 \geq 0$.

(2) If $B_0 < D$ or $B_0 > D, A_0^2 < 2(B_0 - \sqrt{B_0^2 - D^2})$, it then follows from Lemma 1 that there exists a $\tau_2^* > 0$ such that (u_*, v_*) is linearly stable for $\tau_2 < \tau_2^*$. We have also shown in (1) that $\bigcup_{n \neq 0} \mathcal{T}_n$ is an empty set. Therefore, (u_*, v_*) is stable for $\tau_1 \geq 0$ and $\tau_2 < \tau_2^*$.

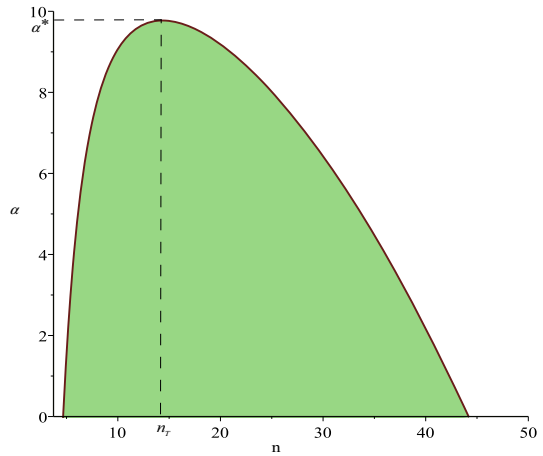
(3) If for some $n \in \mathbb{N} \setminus \{0\}$, either $C_n + D > |B_n|$ or $C_n + D < |B_n|, A_n^2 < 2(B_n - \sqrt{B_n^2 - (C_n + D)^2})$ holds, then from Lemma 6 we know that the stability switching curves \mathcal{T}_n are either closed curves or spiral-like curves or open ended curves. Then, there must exist some (τ_1^0, τ_2^0) and a ω^0 such that $i\omega^0$ is a simple root of $a^n(\lambda; \tau_1^0, \tau_2^0) = 0$. If further $\omega^0(\tau_1^0 - \tau_2^0) \neq k\pi$ ($k \in \mathbb{Z}$), i.e., $\sin(\omega^0(\tau_1^0 - \tau_2^0)) \neq 0$, then according to the curves \mathcal{T}_n , we can determine the stable region Θ of (u_*, v_*) and it is nonempty. □

5 Numerical simulations

Throughout this section, we always fix the parameters

$$\begin{aligned}
 l = 25, \quad r = 1.8, \quad d = 0.01, \quad a = 0.1, \quad p = 0.7, \\
 c = 0.5, \quad m = 0.15, \quad q = 0.66, \quad d_1 = 0.1,
 \end{aligned}
 \tag{74}$$

Fig. 1 (Color online) A graph of $\alpha = \alpha(n^2)$ in n - α plane. The green region is unstable region of (u^*, v^*) . Here $k = 0.1$, $d_2 = 30$, $\tau_1 = 0$ and $\tau_2 = 0$, other parameter values are the same as in (74)



and vary α , τ_1 , τ_2 , k and d_2 to observe the influence of memory-based diffusion, spatial memory, pregnancy cycle and predator-induced fear on the spatial distribution of the prey population. Similar pattern structures can also be seen for the predators.

5.1 The effect of memory-based diffusion on pattern formation

In this subsection, we show the effect of memory-based diffusion on the spatial distribution of prey by assuming $\tau_1 = \tau_2 = 0$ in model (3), i.e., model (1). Besides the parameter values fixed in (74), we take $k = 0.1$ and $d_2 = 30$, then model (3) has a unique positive constant steady state $(u^*, v^*) = (0.8949, 2.7203)$. Our theoretical analysis reveals that (u^*, v^*) can only be destabilized through Turing bifurcation. The instability range is depicted in Fig. 1, from which we know that the critical value of α is $\alpha^* \approx 9.7696$. When $\alpha < 9.7696$, Turing instability occurs and (u^*, v^*) becomes unstable, under this circumstance prey present a nonuniform distribution; while when $\alpha > 9.7696$, (u^*, v^*) remains stable and prey follow the uniform distribution. The numerical simulations shown in Fig. 2 well validate our theoretical analysis. Interestingly, a suitable memory-based diffusion can induce rich spatiotemporal patterns. Prey tend to migrate toward the boundary and the larger α is, the faster prey move to the boundary (Fig. 2(a-c)). These results reveal that small memory-based diffusion may facilitate the occurrence of traveling wave patterns.

5.2 The effect of spatial memory delay on pattern formation

Taking parameter values $k = 0.3$, $d_2 = 10$, $\tau_2 = 0$ and those fixed in (74), in this subsection, we illustrate the influence of spatial memory delay on the spatial distribution of prey by varying τ_1 in model (3). It is easy to compute that model (3) has a unique positive constant equilibrium $(u^*, v^*) = (0.57, 1.96)$ and the critical value of Turing bifurcation is $\alpha^* \approx 1.5654$. In Fig. 3, we select two distinct values of α to conduct the numerical simulations. When $\alpha = 2 > 1.5654$, the critical time delay

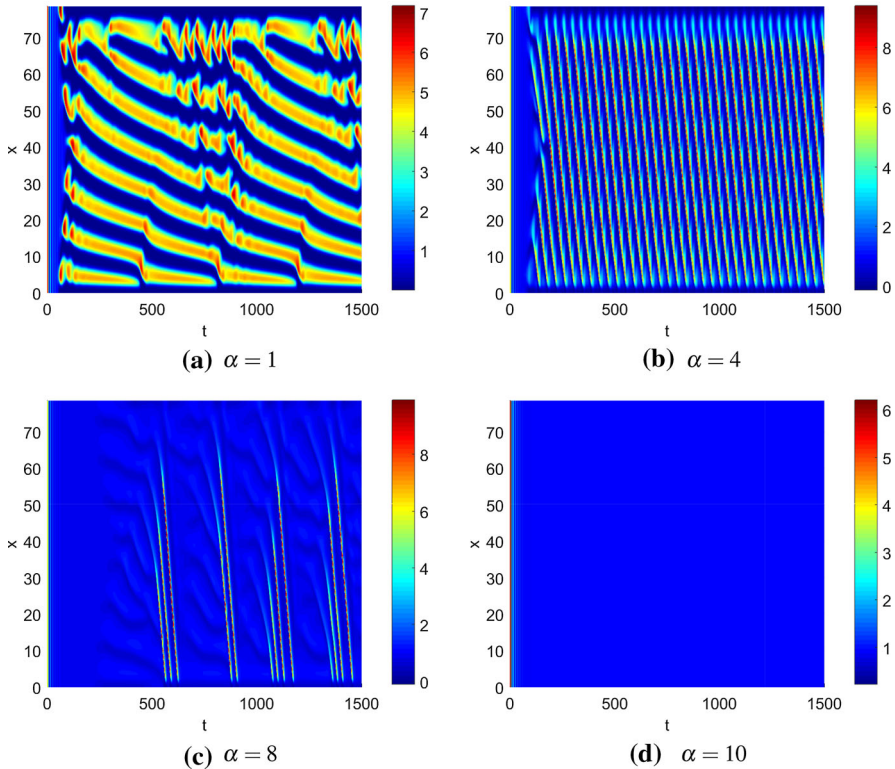


Fig. 2 (Color online) Spatiotemporal diagram of prey for model (3) with the initial functions $u(x, 0) = u^* + 0.0005 \cos(\pi x)$ and $v(x, 0) = v^* + 0.0005 \cos(\pi x)$. The value of α is set as **a** $\alpha = 1$, **b** $\alpha = 4$, **c** $\alpha = 8$, **d** $\alpha = 10$. The other parameters are the same as Fig. 1

of Hopf bifurcation is $\tau_1^* \approx 12.3985$. For $\tau_1 = 5 < 12.3985$, prey follow a uniform distribution (Fig. 3(a)) and for $\tau_1 = 15 > 12.3985$, prey show a spatially nonhomogeneous periodic distribution (Fig. 3(b)). When $\alpha = 0.5 < 1.5654$, Turing instability occurs and prey follow a nonuniform steady state distribution. At this moment, the spatial memory delay may induce the pattern phase transition (Figs. 3(c) and (d)). By comparing Figs. 3(b) and (d), we also find that the memory-based diffusion can induce the emergence of a traveling wave patterns.

Now, we keep the parameter values invariant in Fig. 3(c) and (d) except the diffusion coefficient of the predators d_2 , and increase it from $d_2 = 10$ to 30 to discuss how the spatial memory delay affects the spatial distribution of prey in the case of fast diffusion of the predators. We can compute that the critical value of Turing bifurcation is $\alpha^* \approx 10.8336$. In Fig. 4, $\alpha = 2 < \alpha^*$ and Turing patterns emerge. For small spatial memory delay ($\tau_1 = 1$), flocks of prey migrate towards the boundary of the region at a smaller rate (the slope of each golden area is relatively small), and a small portion of prey will gradually disappear during the evolution process (Fig. 4(a)). If the spatial memory delay is increased a bit ($\tau_1 = 3$), the spatiotemporal distribution of prey becomes a bit chaotic and the density of the prey flocks decreases a bit (Fig. 4(b)). We

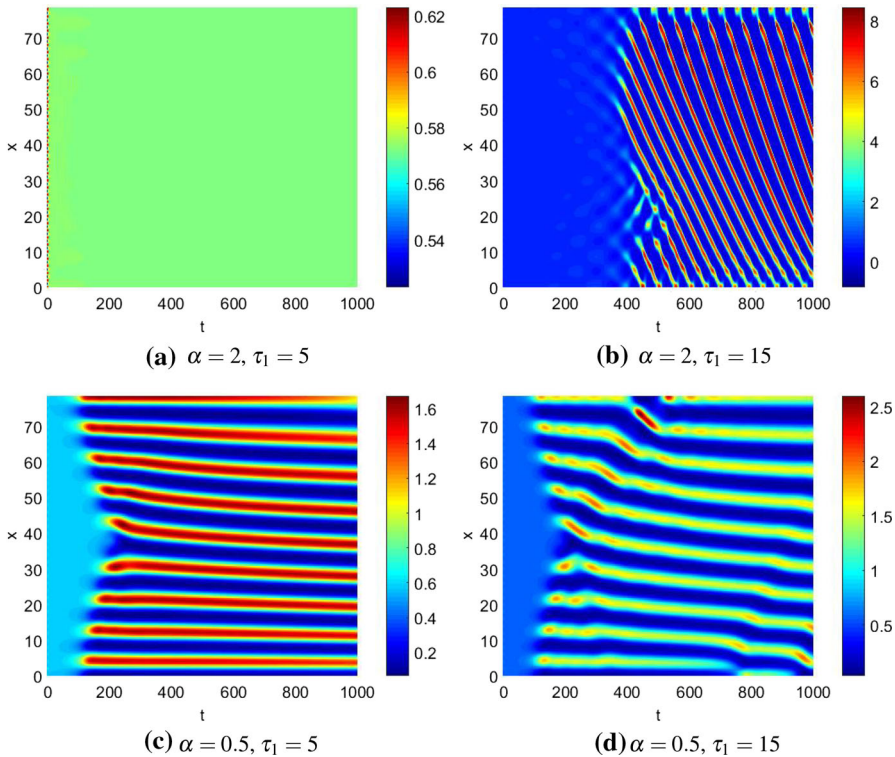


Fig. 3 (Color online) Spatiotemporal diagram of prey for model (3). The initial functions are $u(x, t) = u^* + 10^{-5} \cos(\pi x)$ and $v(x, t) = v^* + 10^{-5} \cos(\pi x)$ for $t \in [-\tau_2, 0]$. The value of τ_2 is set as **a** $\alpha = 0.5$, $\tau_1 = 5$, **b** $\alpha = 0.5$, $\tau_1 = 15$, **c** $\alpha = 2$, $\tau_1 = 5$, **d** $\alpha = 2$, $\tau_1 = 15$. Here $k = 0.3$, $d_2 = 10$ and $\tau_2 = 0$, other parameter values are the same as in (74)

continue to increase the spatial memory delay to $\tau_1 = 5$, the number of prey flocks increase, but we are surprised to find that the prey population evolves according to some interesting laws (Fig. 4(c)). Here, the interaction of the prey population and the predator population still plays a very important role. In general, neither the prey population nor the predator population really presents a periodic oscillation distribution, but at some specific locations, for example, $x = 35$, two populations exhibit seemingly temporal periodicity (Fig. 5(a)), but no spatial periodicity (Fig. 5(b)). In Fig. 5(a), the densities of prey and the predators are neither synchronous nor anti-synchronous: when the density of prey is the smallest or the largest, the density of the predator is the smallest, but when the prey density is some intermediate value, the predator density reaches the maximum. For large spatial memory delay, the prey population presents a regular oscillation distribution, and the oscillation frequency decreases with the increase of memory delay (Figs. 4(d),(e) and (f)). Moreover, by comparing the results in Figs. 5(b) and (d), we can find that with the increase of spatial memory delay, the densities of the prey and predator populations become more regular, and even show some certain synchronization when $\tau_1 = 40$.

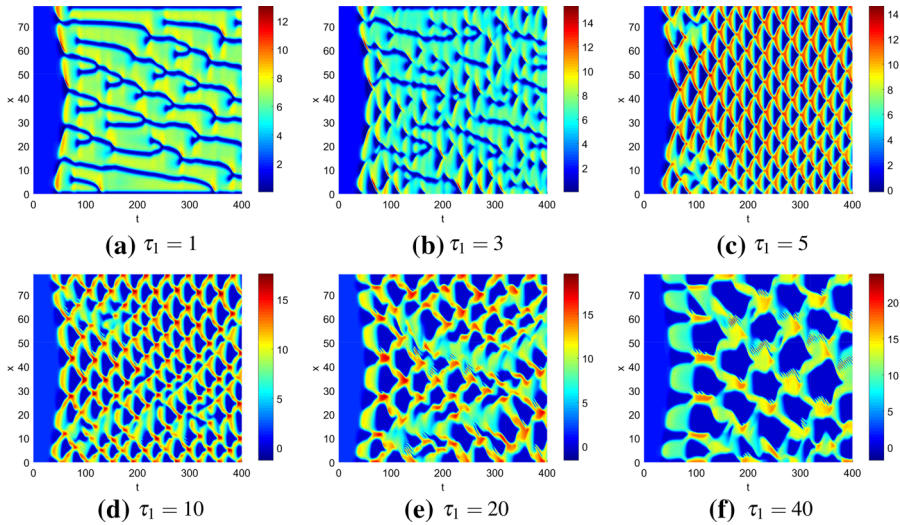


Fig. 4 (Color online) Spatiotemporal diagram of prey for model (3) with the initial functions $u(x, t) = u^* + 10^{-5} \cos(\pi x)$ and $v(x, t) = v^* + 10^{-5} \cos(\pi x)$ for $t \in [-\tau_1, 0]$. The value of τ_1 is set as **a** $\tau_1 = 1$, **b** $\tau_1 = 3$, **c** $\tau_1 = 5$, **d** $\tau_1 = 10$, **e** $\tau_1 = 20$, **f** $\tau_1 = 40$. Here $k = 0.01$, $d_2 = 30$, $\alpha = 2$ and $\tau_2 = 0$, other parameter values are the same as in (74)

5.3 The effect of pregnancy delay on pattern formation

In this subsection, we discuss the influence of pregnancy delay τ_2 on the spatial distribution of prey by taking $k = 1$, $d_2 = 30$, $\tau_2 = 0$ and those parameter values fixed in (74). In this case, model (3) has a unique constant positive steady state $(u^*, v^*) = (0.3333, 1.2570)$, and the critical value of Turing instability is $\alpha^* \approx 3.6538$. In what follows, we take two different values of α to achieve our goal.

We first take $\alpha = 2$, which is smaller than α^* . In this case, Turing instability occurs and (u^*, v^*) is unstable for model (3). Lemma 2 indicates that model (3) exists non-constant steady state solutions. The numerical results shown in Fig. 6 well validate the theoretical analysis. To uncover the influence of τ_2 on the prey population under this condition, we choose four different values of τ_2 to show the pattern results. For small pregnancy delay of prey ($\tau_2 = 1$), prey follow a spatial non-uniform steady state distribution (Fig. 6(a)). When τ_2 is increased, for example $\tau_2 = 3$ or 5, prey eventually present a spatial non-uniform distribution with temporal oscillations, and before arriving this state, prey have a spatially homogeneous distribution for a period of time (Figs. 6(b) and (c)). For large pregnancy delay of prey ($\tau_2 = 10$), prey directly transit from spatial uniform steady-state distribution to spatial non-uniform distribution with temporal oscillation. These results indicate that for prey, its own pregnancy cycle can induce the emergence of spatial non-uniform distribution with temporal oscillation mode.

Then, we take $\alpha = 5.5$, which is larger than α^* . In this case, Turing instability do not occur and the critical value of Hopf bifurcation is $\tau_2^* \approx 1.7265$, which is taken when $n = 0$. Therefore, in addition to the steady state distribution, model (3) can

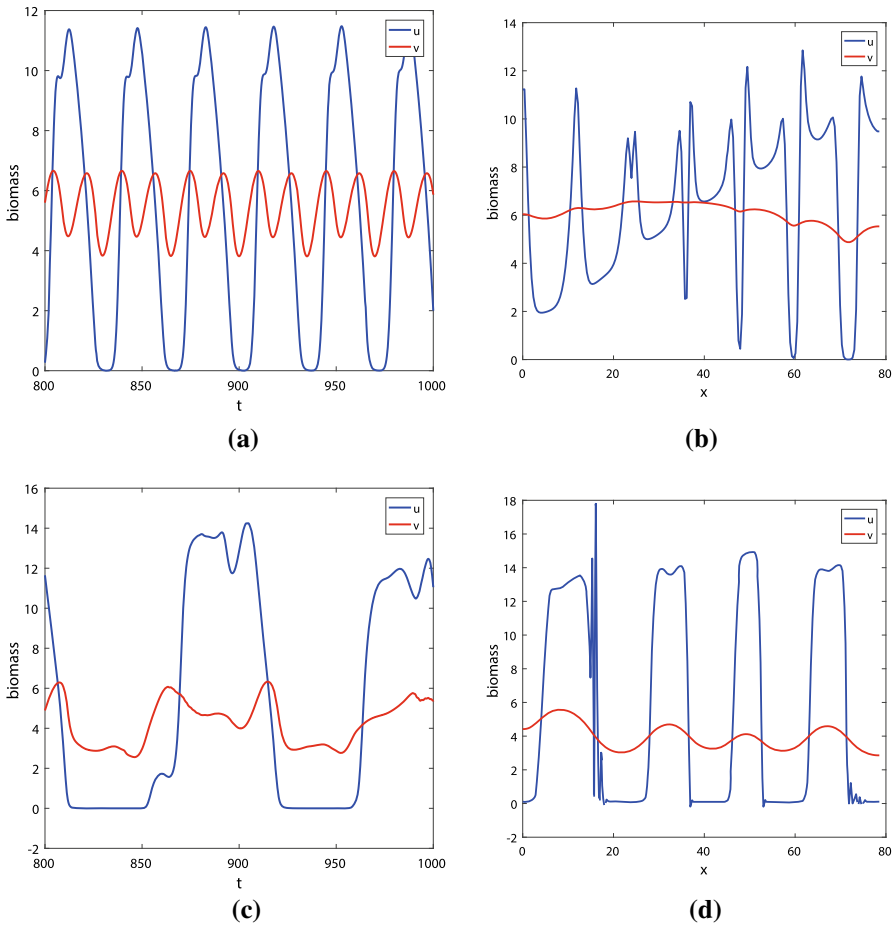


Fig. 5 (Color online) Distributions of prey and predators for model (3). **(a,c)**: the time series diagram at position $x = 35$; **(b,d)**: the spatial distribution at time $t = 1000$. The value of τ_1 is set as **(a,b)** $\tau_1 = 5$, **(c,d)** $\tau_1 = 40$. The initial functions and the other parameters are the same as Fig. 4

only have spatially homogeneous periodic solutions. Our numerical results shown in Fig. 7 well validate the theoretical analysis. When $\tau_2 = 1 < 1.7265$, prey follow the uniform distribution for (Fig. 7(a)) and when $\tau_2 = 3 > 1.7265$, prey present a spatially homogeneous periodic distribution (Fig. 7(b)). In fact, according to the above analysis, we know that this pattern phase transition is completely induced by Hopf bifurcation. However, the pattern phase transition between Figs. 6(a) and 7(a) or Figs. 6(b) and 7(b) is caused by Turing bifurcation.

5.4 $\tau_1 > 0, \tau_2 > 0$

This subsection is devoted to illustrating the joint effect of τ_1 and τ_2 . Take $k = 1, d_2 = 30$ and $\alpha = 5.5$, other parameter values are given in (74). Then model (3) has

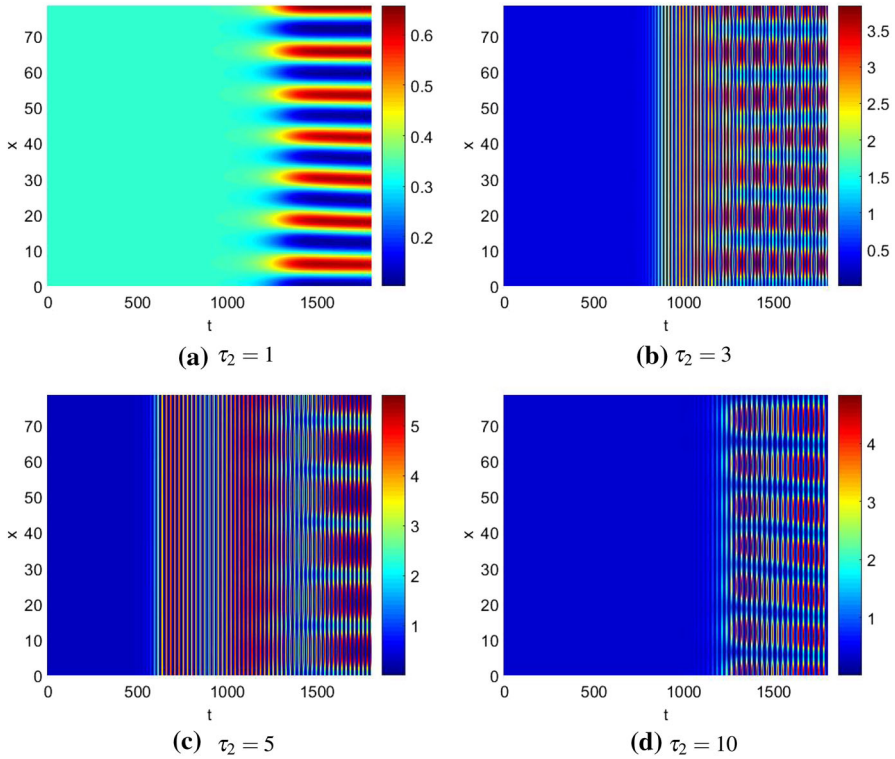


Fig. 6 (Color online) Spatiotemporal diagram of prey for model (3) with $\alpha = 2$. The initial functions are $u(x, t) = u^* + 10^{-5} \cos(\pi x)$ and $v(x, t) = v^* + 10^{-5} \cos(\pi x)$ for $t \in [-\tau_2, 0]$. The value of τ_2 is set as **a** $\tau_2 = 1$, **b** $\tau_2 = 3$, **c** $\tau_2 = 5$, **d** $\tau_2 = 10$. Here $k = 1$, $d_2 = 30$ and $\tau_1 = 0$, other parameter values are the same as in (74)

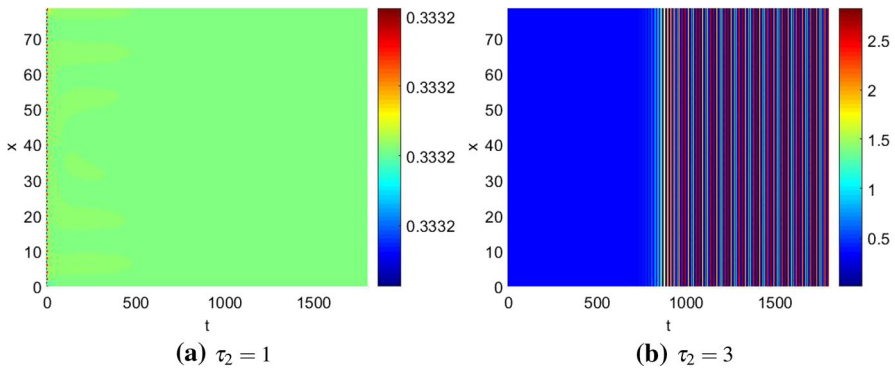


Fig. 7 (Color online) Spatiotemporal diagram of prey for model (3) with $\alpha = 5.5$. The initial functions are $u(x, t) = u^* + 10^{-5} \cos(\pi x)$ and $v(x, t) = v^* + 10^{-5} \cos(\pi x)$ for $t \in [-\tau_2, 0]$. The value of τ_2 is set as **a** $\tau_2 = 1$, **b** $\tau_2 = 3$. The other parameters are the same as Fig. 6

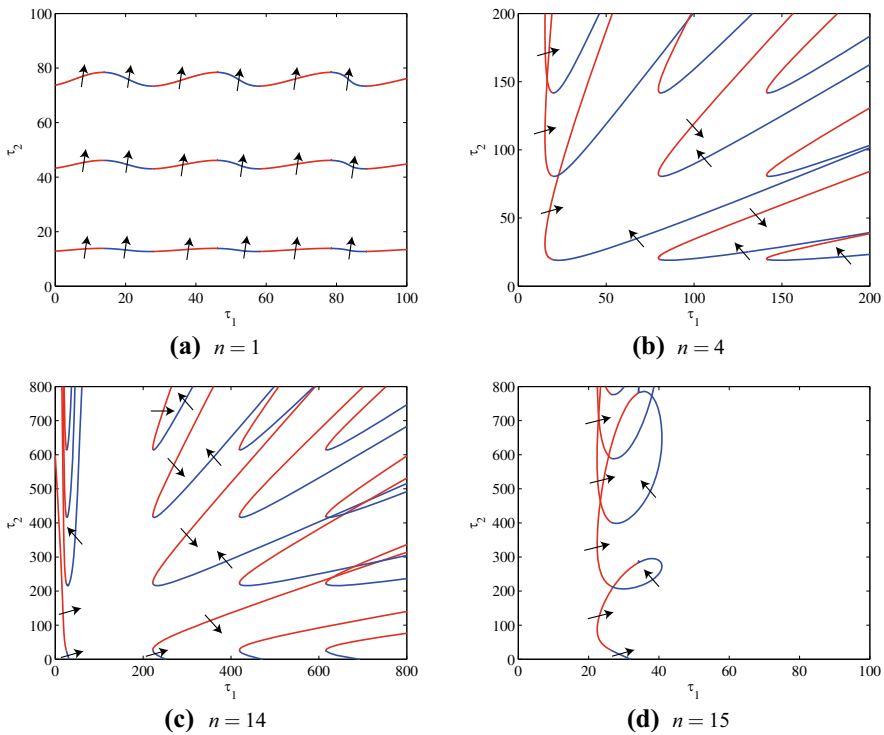


Fig. 8 (Color online) Three types of stability switching curves for different n values. **a** Spiral-like curves with axes oriented τ_1 -axis ($n = 1$). **b** Open ended curves ($n = 4$). **c** Open ended curves ($n = 14$). **d** Spiral-like curves with axes oriented τ_2 -axis ($n = 15$). The blue (red) curve represents $\mathcal{T}_{n,k_1,k_2}^{+k}$ ($\mathcal{T}_{n,k_1,k_2}^{-k}$) and the arrow represents the crossing direction. Here $k = 1$, $d_2 = 30$ and $\alpha = 5.5$, other parameter values are the same as in (74)

a unique positive constant steady state $(u^*, v^*) = (0.3333, 1.2570)$, and the critical value of Turing bifurcation is $\alpha^* \approx 3.6538$, which indicates that (u^*, v^*) is linearly stable for model (3) with $\tau_1 = \tau_2 = 0$. By direct calculations, we find that the crossing set Ω_n is an empty set except $n = 0, 1$ and $3 \leq n \leq 26$. When $n = 0$, model (3) has a single time delay τ_2 , and in this situation, the critical value of Hopf bifurcation is $\tau_2^* \approx 1.7265$. For other n , according to Lemma 6, there are three types of stability switching curves \mathcal{T}_n as shown in Fig. 8: (i) when $n = 1, 5$, \mathcal{T}_n is a series of spiral-like curves with axes oriented τ_1 -axis; (ii) when $15 \leq n \leq 25$, \mathcal{T}_n is a series of spiral-like curves with axes oriented τ_2 -axis; (iii) when $n = 3, 4, 26$ or $6 \leq n \leq 14$, \mathcal{T}_n is a series of open ended curves. In what follows, we select several representative values of n to discuss the structures of stability switching curves \mathcal{T}_n and then determine the linearly stable region of (u^*, v^*) .

When $n = 1$, the crossing set is $\Omega_1 = \Omega_{1,1} \cup \Omega_{1,2} = [0.194, 0.2075] \cup [0.373, 0.381]$. Then the stability switching curves are $\mathcal{T}_1 = \mathcal{T}_1^1 \cup \mathcal{T}_1^2$. According to Lemma 6, we know that both \mathcal{T}_1^1 and \mathcal{T}_1^2 have the form of a series of spiral-like curves with axes oriented τ_1 -axis. In Fig. 8(a), we just show the structure of \mathcal{T}_1^1 .

Specifically, at the left end $\omega = 0.194$, $\mathcal{T}_{1,k_1+1,k_2}^{-1}$ connects $\mathcal{T}_{1,k_1+1,k_2}^{+1}$ and at the right end $\omega = 0.2075$, the other end of $\mathcal{T}_{1,k_1,k_2}^{+1}$ connects $\mathcal{T}_{1,k_1+1,k_2}^{-1}$ and so on. By judging the direction of the curves, it is clear that above each spiral-like curve, Equation (10) has characteristic roots with positive real parts. Therefore, if (τ_1, τ_2) lies in the region below the bottom curve in Fig. 8(a), the equilibrium (u^*, v^*) is stable, and it is unstable if (τ_1, τ_2) is seated above the bottom curve.

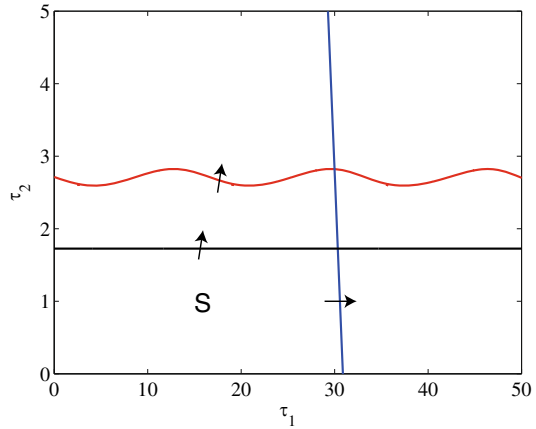
When $n = 4$, the crossing set is $\Omega_4 = \Omega_{4,1} = (0, 0.103]$. Then the stability switching curves are $\mathcal{T}_4 = \mathcal{T}_4^1$, which is a series of open ended curves with both ends extending to infinity, which is formed by connecting $\mathcal{T}_{4,k_1,k_2}^{+1}$ and $\mathcal{T}_{4,k_1,k_2}^{-1}$ at the right end $\omega = 0.103$. The structures of \mathcal{T}_4^1 are shown in Fig. 8(b). Under this circumstance, we know that in the sector domain formed by $\mathcal{T}_{4,k_1,k_2}^{+1}$ and $\mathcal{T}_{4,k_1,k_2}^{-1}$ for fixed k_1, k_2 , Equation (10) has characteristic roots with positive real parts. In other words, the sector regions are all unstable regions. The stable region is enclosed by τ_1 - and τ_2 -axis and the curves \mathcal{T}_4 , but not including \mathcal{T}_4 .

When $n = 14$, the crossing set is $\Omega_{14} = \Omega_{14,1} = (0, 0.032]$. Then the stability switching curves are $\mathcal{T}_{14} = \mathcal{T}_{14}^1$, which is a series of open ended curves with both ends extending to infinity, see Fig. 8(c). As discussed for $n = 4$, the stable region is enclosed by τ_1 - and τ_2 -axis and the curves \mathcal{T}_{14} , but not including \mathcal{T}_{14} .

When $n = 15$, the crossing set is $\Omega_{15} = \Omega_{15,1} = [0.0123, 0.0335]$. Then the stability switching curves are $\mathcal{T}_{15} = \mathcal{T}_{15}^1$, which has the form of a series of spiral-like curves with axes oriented τ_2 -axis. The structures of \mathcal{T}_{15}^1 is shown in Fig. 8(d). Especially, at the right end $\omega = 0.0335$, $\mathcal{T}_{15,k_1,k_2}^{+1}$ connects $\mathcal{T}_{15,k_1,k_2}^{-1}$ and at the left end $\omega = 0.0123$, the other end of $\mathcal{T}_{15,k_1,k_2}^{-1}$ connects $\mathcal{T}_{15,k_1,k_2+1}^{+1}$, and so on. From the crossing direction, we know that on the right hand of each spiral-like curve, Equation (10) has characteristic roots with positive real parts. Therefore, the stable region is enclosed by τ_1 - and τ_2 -axis and the leftmost curve but not including it, see Fig. 8(d).

According to the stability switching curves discussed as above, we can determine the Hopf bifurcation curve in τ_1 - τ_2 plane by plotting the stability switching curves for each n , which is shown in Fig. 9. The stable region of (u^*, v^*) is marked by S , in which Hopf bifurcation cannot occur. As (τ_1, τ_2) moves and crosses the black curve (or blue curve), the equilibrium (u^*, v^*) loses its stability. We show some numerical results in Fig. 10 to reveal the joint influence of τ_1, τ_2 on the spatial distribution of prey by selecting four sets delay values. For $\tau_1 = 5, \tau_2 = 1.5$, the delay pair (τ_1, τ_2) lies in the stable region and the positive equilibrium (u^*, v^*) is stable. In this case, prey follow the uniform distribution (see Fig. 10(a)). We first keep $\tau_1 = 5$ invariant and increase τ_2 such that (τ_1, τ_2) is above the stable region, for example, $\tau_1 = 5, \tau_2 = 5$, in this situation, prey show a spatially homogeneous periodic distribution (see Fig. 10(b)). In fact, this is because the black curve stands for Hopf bifurcation curve for $n = 0$, which indicates that only spatially homogeneous periodic solutions can emerge. Now we keep $\tau_2 = 1.5$ invariant and increase τ_1 such that (τ_1, τ_2) is on the right side of the blue curve, for example, $\tau_1 = 31, \tau_2 = 1.5$, under this circumstance, prey show a spatially nonhomogeneous periodic distribution (see Fig. 10(c)). This phase transition is because (τ_1, τ_2) crosses the blue curve, which corresponds to the stability switching

Fig. 9 (Color online) Hopf bifurcation curves in τ_1 - τ_2 plane. The stable region is marked by S. Different color curves stand for stability switching curves when n takes different values. Red curve ($n = 1$), Blue curve ($n = 12$), Black curve ($n = 0$). The arrow represents the crossing direction. The parameters take the same values as Fig. 8



curve for $n = 12$. When (τ_1, τ_2) is seated in the upper right region of the stable region, prey present a spatially nonhomogeneous distribution (see Fig. 10(d)).

5.5 The effect of fear level on pattern formation

It is known that the average pregnancy period can almost be regarded as a fixed constant for a species. For this reason, we fix $\tau_2 = 5$. As stated in the introduction, Zanette et al. (2011) pointed out that the predator-induced fear can reduce the birth rate and increase the mortality rate of prey. The predator’s attack speed needs to be large enough to make prey feel fear, otherwise, the fear will not affect the prey-predator dynamics significantly. In Fig. 11, we discuss the effect of fear on the spatial distribution of prey by varying the fear level k without considering the memory ability of prey. We can observe the transitions from uniform stationary distribution to nonuniform distribution to spatially nonhomogeneous periodic distribution and finally to stationary distribution. If the predator-induced stress is removed ($k = 0$), the prey population follows the stationary distribution (Fig. 11(a)). For small fear level, for example, $k = 0.005$ or $k = 0.01$, the prey population tends to move to the boundary as time evolves (Figs. 11(b) and (c)). As k increases gradually, prey distribute in fragments in space, but the distribution of prey is still relatively regular (Figs. 11(d) and (e)). When we increase k continuously until $k = 0.3$ (or $k = 0.5$), we are surprised to see that prey follow a seemingly spatially nonhomogeneous periodic distribution (Figs. 11(f) and (g)). If we continue to increase k (e.g., $k = 1$), the spatially homogeneous periodic distribution disappears gradually and the spatially nonhomogeneous periodic distribution eventually emerges (Fig. 11(h)). However, if k is large enough ($k = 10$), the uniform distribution reappears (Fig. 11(i)).

In addition, we show the relations between the amplitude of the average prey density and the fear level in Fig. 12. Here, the average density refers to the spatial average over the whole region, that is, the biomass of the whole area divided by the size of the area. It means that the amplitude of prey density is negatively correlated with fear intensity. The constant positive steady state of model (3) is linearly stable if the fear

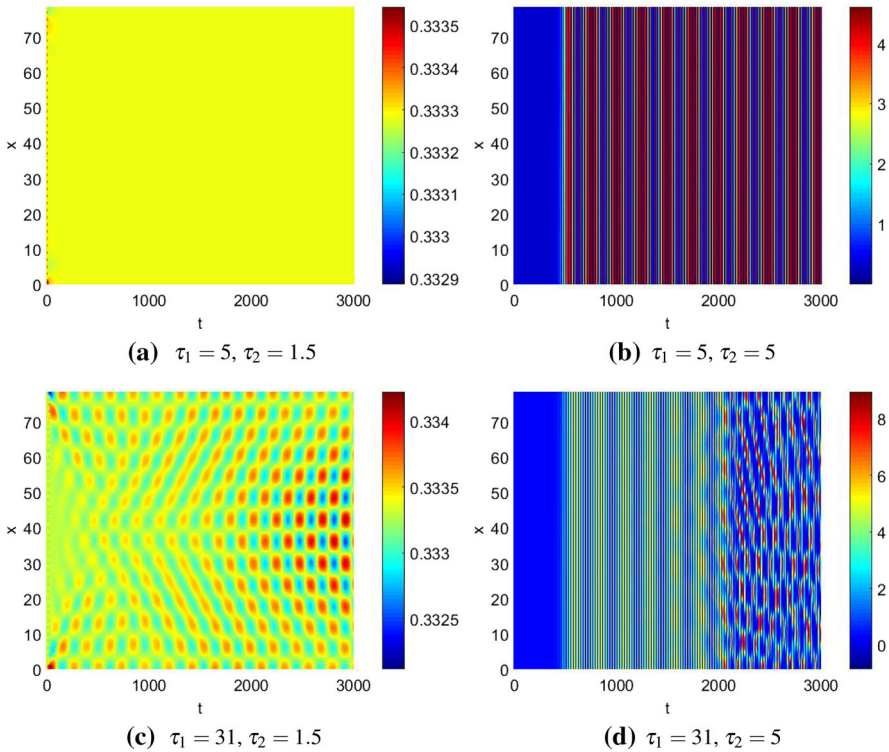


Fig. 10 (Color online) Spatiotemporal diagram of prey for model (3). The initial functions are $u(x, t) = u^* + 10^{-5} \cos(\pi x)$ and $v(x, t) = v^* + 10^{-5} \cos(\pi x)$ for $t \in [-\tau_2, 0]$. The value of τ_2 is set as (a) $\tau_2 = 1$, (b) $\tau_2 = 3$, (c) $\tau_2 = 5$, (d) $\tau_2 = 10$. The other parameters take the same values as Fig. 8

intensity is smaller or larger, but if the fear intensity is moderate, it becomes unstable and a temporal oscillation solution emerges.

6 Discussion

In this paper, we propose and analyze a spatial memory prey-predator model with predator avoidance and pregnant time delay, in which the direct predation is described by Holling type II functional response and the indirect effect of predation is presented by the fear function. The average pregnancy period of prey is denoted as τ_2 . We assume that the pregnant prey do not move during their pregnancy cycle, which indicates that during the pregnancy, prey tend to stay in one safe location to avoid the threat of predators. This assumption sounds reasonable and makes the model “correct” to piece up delay and diffusion, whose combination normally has issues as we know. In addition, the startled prey always make a conscious effort to avoid the predators and then a directional movement is formed (called predator-taxis), which is described by the memory-based diffusion term. The indirect effect of predation may have a more

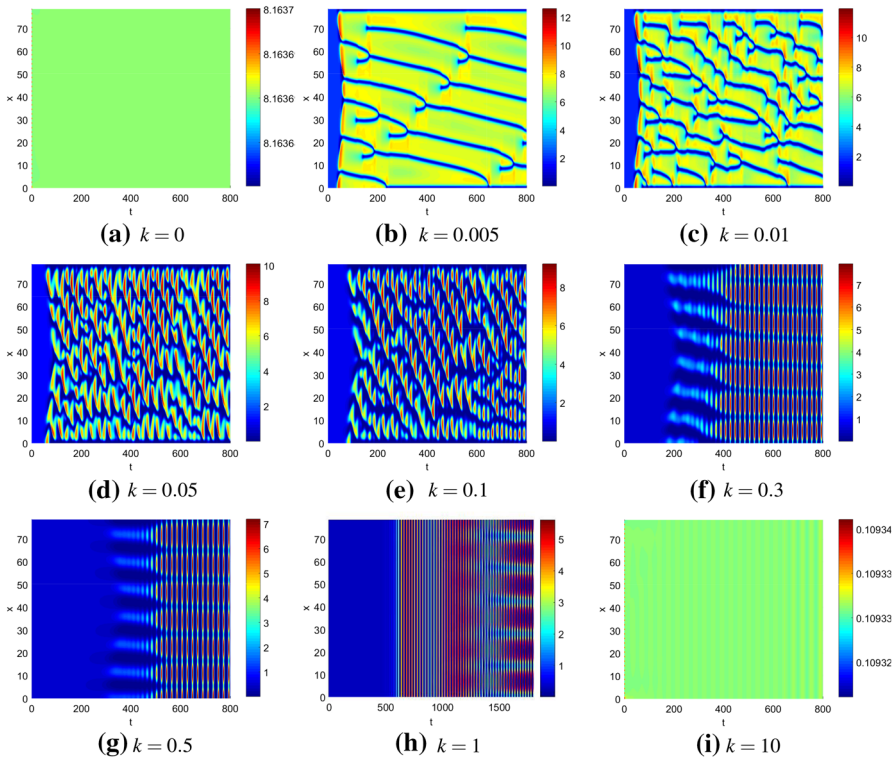


Fig. 11 (Color online) Spatiotemporal diagram of prey for model (3). The initial functions are $u(x, t) = u^* + 10^{-5} \sin(\pi x)$ and $v(x, t) = v^* + 10^{-5} \sin(\pi x)$ for $t \in [-\tau_2, 0]$. The value of k is set as **a** $k = 0$, **b** $k = 0.005$, **c** $k = 0.01$, **d** $k = 0.05$, **e** $k = 0.1$, **f** $k = 0.3$, **g** $k = 0.5$, **h** $k = 1$, **i** $k = 10$. Here $d_2 = 30$, $\tau_1 = 0$, $\tau_2 = 5$ and $\alpha = 2$, other parameter values are the same as in (74)

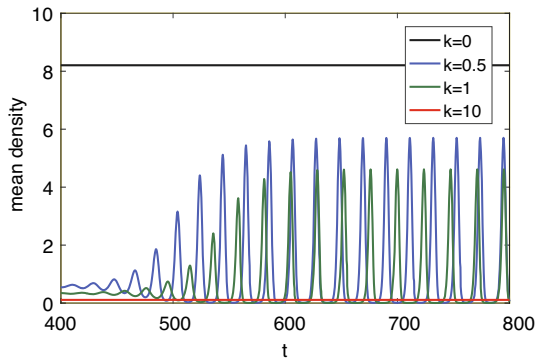


Fig. 12 (Color online) The time series diagram of the mean density of prey for model (3). The initial functions are $u(x, t) = u^* + 10^{-5} \sin(\pi x)$ and $v(x, t) = v^* + 10^{-5} \sin(\pi x)$ for $t \in [-\tau_2, 0]$. The value of k is set as $k = 0$ (black curve), $k = 0.5$ (blue curve), $k = 1$ (green curve), $k = 10$ (red curve). The other parameter values are the same as Fig. 11

striking effect on prey than the direct predation. Undoubtedly, the severity of this indirect effect can be influenced by some characteristics of prey, such as, the memory-based diffusion coefficient, the memory period, the pregnancy period and the natural birth rate. It is important to uncover the impact of these factors on the prey distribution over space and time.

For the subject model (3), in this paper, we focus on the situation when it exists a stable positive constant steady state (u^*, v^*) . In the absence of spatial memory and pregnancy period, model (3) is reduced to model (1), which has ever been studied numerically in Wang and Zou (2018). Both our theoretical and numerical results reveal that slow memory-based diffusion can induce a Turing instability, which makes (u^*, v^*) lose its stability and consequently a spatially non-uniform steady state emerges, while fast memory-based diffusion does not affect the stability of (u^*, v^*) . This is consistent with the universal conclusion that fast diffusion tends to homogenize.

In the presence of spatial memory only, model (3) is reduced to model (2). In this case, spatially homogeneous periodic solutions can not occur. For fast memory-based diffusion, there is a critical spatial memory delay. When the spatial memory delay is less than this critical value, the positive constant steady state (u^*, v^*) is stable and the prey population is uniformly distributed; when the spatial memory delay exceeds this critical value, (u^*, v^*) loses its stability, the prey population presents a spatially inhomogeneous periodic distribution. For slow memory-based diffusion, (u^*, v^*) is unstable and the population presents a spatially non-uniform distribution due to Turing instability. In this situation, as illustrated in Fig. 4, the spatial memory delay may cause various spatial distribution structures of the prey population. Particularly, large spatial memory delay can induce a regular oscillation distribution and the oscillation frequency decreases with the increase of memory delay (see Figs. 4(d),(e) and (f)).

In the presence of pregnant time delay only, the prey population with fast memory-based diffusion and long pregnancy cycles is more easy to show a periodic distribution in time, which is either spatially homogeneous or nonhomogeneous. Whether the solution is spatially uniform or not depends on whether the minimum critical delay for the occurrence of Hopf bifurcation is achieved when n is zero or not. In Fig. 7(b), we show a numerical result which distribution is spatially homogeneous periodic. While the prey population with slow memory-based diffusion presents a spatially nonuniform distribution, which is mainly caused by Turing instability. Also, the individuals with long pregnancy cycles show some temporal heterogeneity (see Fig. 6). Moreover, for a specific prey species, its pregnancy period can be regarded as a constant. When prey are threatened, they instinctively consume less food or adjust strategies to escape danger in order to find a suitable 'refuge'. The effects of different levels of fear on prey will vary greatly. A suitable level of fear may cause fragmentation or regular spatiotemporal periodic distribution of prey (see Fig. 11).

For the model with both the two delays, the structures of the stability switching curves for each feasible n can be determined by using the method in Gu et al. (2005), which are either spiral-like curves or open-ended curves (see Fig. 8). The bifurcation diagram in Fig. 9 indicates that both the spatial memory delay and the pregnancy cycle of prey may induce the instability of the positive constant steady state (u^*, v^*) . The dynamics of the model with two delays are much richer than those with single one: the prey population may exhibit a spatially homogeneous or nonhomogeneous peri-

odic distribution (induced by Hopf bifurcation), or simply spatially nonhomogeneous distribution (see Fig. 10).

As we have argued above, pattern formation can be affected by many factors involved in the model under consideration, such as the reproduction rate, the diffusion rate and the memory-based diffusion rate. In fact, under the background of global climate change, the richness of species, species distribution pattern, inter-specific relationship will undergo profound changes, and thereby increase the risk of species invasion and species extinction. The adaptive ability of a species will affect its survival. Recently, Sommers and Chesson (2019) indicated that both the adaptive ability and predator avoidance behavior can determine the destiny of species. The investigation of a prey-predator model incorporating both the adaptive behavior of the species and the indirect effect of predation will remain an interesting and ongoing topic.

Acknowledgements The authors would like to thank the two anonymous referees for their valuable comments and suggestions which have greatly improved this paper.

Declarations

Conflict of interest The authors declare that they have no conflict of interest.

References

- An Q, Beretta E, Kuang Y, Wang C, Wang H (2019) Geometric stability switch criteria in delay differential equations with two delays and delay dependent parameters. *J Diff Equ* 266(11):7073–7100
- An Q, Wang C, Wang H (2020) Analysis of a spatial memory model with nonlocal maturation delay and hostile boundary condition. *Disc Continuous Dyn Syst* 40(10):5845–5868
- Clinchy M, Sheriff MJ, Zanette LY, Boonstra R (2013) Predator-induced stress and the ecology of fear. *Funct Ecol* 27(1):56–65
- Cooke KL, Den Driessche PV (1996) Analysis of an seirs epidemic model with two delays. *J Math Biol* 35(2):240–260
- Du Y, Niu B, Wei J (2019) Two delays induce hopf bifurcation and double hopf bifurcation in a diffusive leslie-gower predator-prey system. *Chaos* 29(1):013101
- Fagan WF, Lewis MA, Augermethe M, Avgar T, Benhamou S, Breed GA, Ladage LD, Schlager UE, Tang W, Papastamatiou YP et al (2013) Spatial memory and animal movement. *Ecol Lett* 16(10):1316–1329
- Gu K, Niculescu S, Chen J (2005) On stability crossing curves for general systems with two delays. *J Math Anal Appl* 311(1):231–253
- Jackson M, Chencharpentier BM (2017) Modeling plant virus propagation with delays. *J Comput Appl Math* 309:611–621
- Jia D, Zhang T, Yuan S (2019) Pattern dynamics of a diffusive toxin producing phytoplankton-zooplankton model with three-dimensional patch. *Int J Bifurc Chaos* 29(4):1930011
- Kumar A, Dubey B (2019) Modeling the effect of fear in a prey-predator system with prey refuge and gestation delay. *Int J Bifurc Chaos* 29(14):1950195
- Lin X, Wang H (2012) Stability analysis of delay differential equations with two discrete delays. *Canadian Appl Math Quart* 20(4):519–533
- Martin A, Ruan S (2001) Predator-prey models with delay and prey harvesting. *J Math Biol* 43(3):247–267
- May RM (1973) Time-delay versus stability in population models with two and three trophic levels. *Ecology* 54(2):315–325
- Mondal S, Maiti A, Samanta GP (2018) Effects of fear and additional food in a delayed predator-prey model. *Biophys Rev Lett* 13(04):157–177
- Montagnes DJS, Zhu X, Gu L, Sun Y, Wang J, Horner R, Yang Z (2019) False exclusion: a case to embed predator performance in classical population models. *Am Nat* 194(5):654–670

- Potts JR, Lewis MA (2019) Spatial memory and taxis-driven pattern formation in model ecosystems. *Bull Math Biol* 81(7):2725–2747
- Preisser EL, Bolnick DI, Benard MF (2005) Scared to death? the effects of intimidation and consumption in predator-prey interactions. *Ecology* 86(2):501–509
- Qu Y, Wei J, Ruan S (2010) Stability and bifurcation analysis in hematopoietic stem cell dynamics with multiple delays. *Physica D Nonlinear Phenomena* 239(20):2011–2024
- Ruan S, Wei J (2003) On the zeros of transcendental functions with applications to stability of delay differential equations with two delays. *Dyn Continuous Disc Impuls Syst* 10(6):863–874
- Shi J, Wang C, Wang H (2019) Diffusive spatial movement with memory and maturation delays. *Nonlinearity* 32(9):3188–3208
- Shi J, Wang C, Wang H, Yan X (2020) Diffusive spatial movement with memory. *J Dyn Diff Equ* 32(2):979–1002
- Shi Q, Shi J, Song Y (2017) Hopf bifurcation in a reaction-diffusion equation with distributed delay and dirichlet boundary condition. *J Diff* 263(10):6537–6575
- Shi Q, Shi J, Song Y (2019) Hopf bifurcation and pattern formation in a delayed diffusive logistic model with spatial heterogeneity. *Disc Continuous Dyn Syst-Series B* 24(2):467–486
- Sommers P, Chesson P (2019) Effects of predator avoidance behavior on the coexistence of competing prey. *Am Nat* 193(5):E132–E148
- Song Y, Peng Y, Wei J (2008) Bifurcations for a predator-prey system with two delays. *J Math Anal Appl* 337(1):466–479
- Song Y, Wu S, Wang H (2019) Spatiotemporal dynamics in the single population model with memory-based diffusion and nonlocal effect. *J Diff Equ* 267(11):6316–6351
- Song Y, Peng Y, Zhang T (2021) The spatially inhomogeneous hopf bifurcation induced by memory delay in a memory-based diffusion system. *J Diff Equ* 300:597–624
- Sun G (2016) Mathematical modeling of population dynamics with allee effect. *Nonlinear Dyn* 85(1):1–12
- Travers M, Clinchy M, Zanette L, Boonstra R, Williams TD (2010) Indirect predator effects on clutch size and the cost of egg production. *Ecol Lett* 13(8):980–988
- Wang H, Nagy JD, Gilg O, Kuang Y (2009) The roles of predator maturation delay and functional response in determining the periodicity of predator-prey cycles. *Math Biosci* 221(1):1–10
- Wang X, Zou X (2017) Modeling the fear effect in predator-prey interactions with adaptive avoidance of predators. *Bull Math Biol* 79(6):1325–1359
- Wang X, Zou X (2018) Pattern formation of a predator-prey model with the cost of anti-predator behaviors. *Math Biosci Eng* 15(3):775–805
- Wang X, Zanette L, Zou X (2016) Modelling the fear effect in predator-prey interactions. *J Math Biol* 73(5):1179–1204
- Wang Y, Zou X (2020) On a predator-prey system with digestion delay and anti-predation strategy. *J Nonlinear Sci* 30(4):1579–1605
- Wang YX, Li WT (2019) Spatial patterns of a predator-prey model with beddington-deangelis functional response. *Int J Bifurc Chaos* 29(11):1950145
- Yan S, Jia D, Zhang T, Yuan S (2020) Pattern dynamic in a diffusive predator-prey model with hunting cooperations. *Chaos Solitons Fractals* 130:109428
- Yang J, Yuan S (2021) Dynamics of a toxic producing phytoplankton-zooplankton model with three-dimensional patch. *Appl Math Lett* 118:107146
- Zanette L, White AF, Allen MC, Clinchy M (2011) Perceived predation risk reduces the number of offspring songbirds produce per year. *Science* 334(6061):1398–1401
- Zhang S, Yuan S, Zhang T (2022) A predator-prey model with different response functions to juvenile and adult prey in deterministic and stochastic environments. *Appl Math Comput* 413:126598

Publisher's Note Springer Nature remains neutral with regard to jurisdictional claims in published maps and institutional affiliations.